Finite Element Analysis of Intracranial Pressure under the influence of Brain Tumor

Author

Ali Ahmed

Regn Number

00000206586

Supervisor

Dr. Zartasha Mustansar

DEPARMENT OF BIOMEDICAL ENGINEERING & SCIENCES

SCHOOL OF MECHANICAL & MANUFACTURING ENGINEERING

NATIONAL UNIVERSITY OF SCIENCES AND TECHNOLOGY

ISLAMABAD

September, 2020

Finite Element Analysis of Intracranial Pressure under the influence of Brain Tumor

Author

Ali Ahmed

Regn Number

00000206586

A thesis submitted in partial fulfillment of the requirements for the degree of

MS Biomedical Engineering

Thesis Supervisor:

Dr. Zartasha Mustansar

Thesis Supervisor's Signature: 

DEPARTMENT OF BIOMEDICAL ENGINEERING AND SCIENCES

SCHOOL OF MECHANICAL & MANUFACTURING ENGINEERING

NATIONAL UNIVERSITY OF SCIENCES AND TECHNOLOGY, ISLAMABAD

September, 2020

Declaration

I certify that this research work titled **"*Finite Element Analysis of Intracranial Pressure under the influence of Tumor"*** is my own work. The work has not been presented elsewhere for assessment. The material that has been used from other sources has been properly acknowledged and duly cited. The thesis is submitted with signature of the supervisor (hereinabove) and mine and has been proof-read for errors.

Signature of Student

ALI AHMED

REG NO: 00000206586

Plagiarism Certificate (Turnitin Report)

This thesis has been checked for Plagiarism. Turnitin report endorsed by Supervisor is attached.

Signature of Student

ALI AHMED

REG NO: 00000206586

Signature of Supervisor

DR. ZARTASHA MUSTANSAR

Copyright Statement

- Copyright in text of this thesis rests with the student author. Copies (by any process) either in full, or of extracts, may be made only in accordance with instructions given by the author and lodged in the Library of NUST School of Mechanical & Manufacturing Engineering (SMME). Details may be obtained by the Librarian. This page must form part of any such copies made. Further copies (by any process) may not be made without the permission (in writing) of the author.
- The ownership of any intellectual property rights which may be described in this thesis is vested in NUST School of Mechanical & Manufacturing Engineering, subject to any prior agreement to the contrary, and may not be made available for use by third parties without the written permission of the SMME, which will prescribe the terms and conditions of any such agreement.
- Further information on the conditions under which disclosures and exploitation may take place is available from the Library of NUST School of Mechanical & Manufacturing Engineering, Islamabad.

Acknowledgements

I am thankful to my Creator Allah Subhana-Watala to have guided me throughout this work at every step and for every new thought which You setup in my mind to improve it. Indeed, I could have done nothing without Your priceless help and guidance. Whosoever helped me throughout the course of my thesis, whether my parents or any other individual was Your will, so indeed none be worthy of praise but You.

I am profusely thankful to my beloved parents who raised me when I was not capable of walking and continued to support me throughout in every department of my life.

I would also like to express thanks to my supervisor **Dr. Zartasha Mustansar** for her help throughout my thesis. A special thanks to her for tremendous support and cooperation. Each time I got stuck in something, she came up with the solution. Without her help I would not have been able to complete my thesis. I appreciate her patience and guidance throughout the whole thesis.

I would also like to thank **Dr. Syed Omer Gilani, Dr. Asim Waris** and **Dr Umar Ansari** for being on my thesis guidance and evaluation committee and express my special thanks to them for their help.

It would be great injustice if I do not commend the support staff of logistics and labs of **SMME** and **RCMS** for their support. Notable among others, is the supercomputer assistance provided by **Engineer Muhammad Hassan** of RCMS which helped me a lot in the computing part of my thesis.

Finally, I would like to express my gratitude to all the individuals who have rendered valuable assistance to my study. Notable among them is my colleague **Muhammad Uzair Ul Haq** who rendered invaluable jewels of wisdom.

I dedicate this thesis to my exceptional parents and my brother whose tremendous support and cooperation led me to this wonderful accomplishment.

Abstract

Intracranial pressure (ICP) is an important biomarker in neurosurgical and pathological studies. The stability of ICP is extremely random and unpredictable within the cranium, especially when a pathology is present such as cerebral edema, hematoma or tumor. Since intracranial compartments, i.e., blood, brain and Cerebrospinal fluid (CSF) are nearly incompressible, therefore, any net change in one compartment, such as in the case of brain tumor (whereby total mass of brain increases), induces a corresponding rise in pressure due to compression of volume of another compartment. This pressure-volume relationship is non-linear inter-alia due to an early compliance mechanism provided by CSF. However, after exhaustion of this compliance mechanism, ICP rises drastically. Most studies in literature do provide an analysis and inter-se relationship of ICP biomechanics and pathologies. However, little work is done in modeling ICP correlation, if any, in presence of a growing tumor. This study, in view of the foregoing, attempts to provide a finite-element-based model (FEM) of patient diagnosed with an early stage brain tumor in left temporal region. The model incorporates non-linear ICP dynamics inside the cranium, together-with considering the growing tumor pressures on the brain parenchyma. The proposed computational numerical model exploits the fluid-structure interaction (FSI) modeling technique which is used to include and combine both structural (brain tumor and parenchyma) and fluid (CSF) interactions. Results suggest that there is a considerable influence of tumor in brain damage. The magnitude of this deformation goes up to 5 micrometers which is notable for closed head cases. Magnitude of ICP inside cranium goes up to 1442 Pascals (10.81 mmHg) which, though being under the normal range of ICP (15 mmHg), is still significant considering that since this thesis addresses the case of tumor which is in its early stages. The framework presented in this work can also be beneficial in modeling other cases such as hematoma, cerebral edema etc. The study will also be useful for clinical experts in making informed decisions prior to any surgical intervention.

Key Words: *Intracranial pressure (ICP), intracranial compliance, Cerebrospinal Fluid (CSF), Finite Element method, Image based Modeling.*

Table of Contents

List of Abbreviations

ICP	Intracranial Pressure
MAP	Mean Arterial Pressure
CPP	Cerebral Perfusion Pressure
TBI	Traumatic Brain Injury
MRI	Magnetic Resonance Imaging
WM	White Matter
GM	Gray Matter
CNS	Central Nervous System
PNS	Peripheral Nervous System
SNS	Somatic Nervous System
ANS	Autonomic Nervous System
ENS	Enteric Nervous System
CSF	Cerebrospinal Fluid
GCS	Glasgow Comma Scale
EVD	External Ventricular Drainage
TCD	Transcranial Doppler Ultrasonography
FEM	Finite Element Method
FSI	Fluid Structure Interaction
ROI	Region of Interest
HGG	High Grade Gliomas
LGG	Low Grade Glioma
ALE	Arbitrary Lagrangian Eulerian
PISO	Pressure Implicit with Splitting of Operators
ILU	Incomplete Lower Upper
AMG	Algebraic Multigrid Method
CFL	Courant-Friedrichs-Lewy number

List of Figures

List of Tables

CHAPTER 1—PREAMBLE

1.1 Introduction

Elevated Intracranial Cerebral pressure **(hereinafter to be referred as ICP)** is one of the first problem usually encountered by a neurosurgeon in a clinical emergency. If not treated early, and if the pressure is too high, then it may cause permanent deformation of brain; it can contribute towards Obstructive Hydrocephalus, Ischemic stroke *et cetera*. Given the fact that the measurement of ICP entails using invasive surgical procedures which may not be used routinely in a clinical setting, hence, the clinical problems associated therewith [1] (in invasive measurement) continue to pose a great clinical challenge for the medical community. Likewise, in certain pathophysiological conditions such as Cerebral Edema, Mass lesions (tumor or intracranial hematoma), Traumatic Brain Injury **(TBI)** etc., without having analyzed the mechanics of ICP, a suitable treatment cannot be offered thereon because the subsequent treatment depends on the quantitative measure of ICP. Against this backdrop, the biomedical engineering community has undertaken the task of addressing the aforementioned challenges (both physiological and pathological), and undoubtedly, some of them have indeed been tackled by way of extensive research, and through innovative product designs. However, there is one problem which has not been thoroughly understood and that is: Investigating the biomechanical relationship of ICP under the influence of Brain tumor. This is the question which this dissertation pointedly tries to answer. Furthermore, in a practical situation, since brain tumor has a delayed clinical onset (in terms of its symptoms), therefore it is hypothesized that investigating ICP correlation may improve prognostic potential in terms of early detection and diagnosis of tumor. Forasmuch as invasive techniques cannot be used, whence it is imperative to develop a computer model. There are two parts of the computational model, (1) Data acquisition, Segmentation and 3D Reconstruction of MRI **(Magnetic Resonant Imaging)** scans, and (2) 3D Volumetric meshing and Structural analyses under different loading conditions. For former, Image-based Modelling is used and for the latter Finite Element Method **(hereinafter referred to as FEM)** is incorporated which is popular in discretizing any intricate geometry into mesh elements (to the required size). This enables us to apply complex partial differential equations on each elemental domain and hence find the solution to the required accuracy and repeatability.

1.2 Motivation

According to statistical report published by Central brain tumor registry of the United States [2], the five-year survival rate in US for patients with all malignant brain tumors from 2001-2015 was only 8% from diagnosed 34.8% male and 37.1% female patients. While for most aggressive and malignant tumor such as glioblastoma, the five-year survival rate is only 6.8%. To elaborate further, according to another survey [3] about 23,890 adults in the United States of America will be diagnosed with brain cancers this year. Clinically challenging effects of brain tumor inter-alia include stroke, ischemia, elevated intracranial pressures (ICP), obstruction to flow the of Cerebrospinal fluid (CSF) et cetera. Biomechanical modelling of CSF in view of aforenoted is one of the important factors which merits investigation because it is directly or indirectly linked to aforementioned effects. To put into perspective, according to another statistic report published by (Hydrocephalus Association [4]), every year about a million Americans will be affected by Hydrocephalus (excessive retention of CSF in ventricles), which among other things is also induced by stenosis of cerebral aqueduct due to compressive forces of brain tumor. For instance, abrupt change in CSF velocity in the cerebral aqueduct due to stenosis may result into seizures, gait imbalance, visual problems, obstructive hydrocephalus et cetera. Therefore, it is imperative, and necessary, to describe by means of a numerical model the underlying interactions of CSF flow with the ventricular walls which is critical in developing towards anatomically realistic biomechanical model of CSF. The focus of this investigation would thus revolve around developing a complete biomechanical model of CSF in brain ventricles which may further aid clinicians and practitioners in taking informed decisions before undertaking any surgical intervention. It is also important to note that in patients having complaint of elevated ICP problem, the leading is the excessive or obstruction to the flow of CSF [1] which makes it all the more necessary to develop anatomically realistic biomechanical model of CSF flow in ventricles in general and for brain tumor case in particular. Figure 1[1] (next page) shows some of the effects of increased ICP on human body.

[1] [1] Picture taken, and publicly available, from the following link <https://www.ausmed.com/cpd/articles/increased-intracranial-pressure> accessed 15th August 2019.

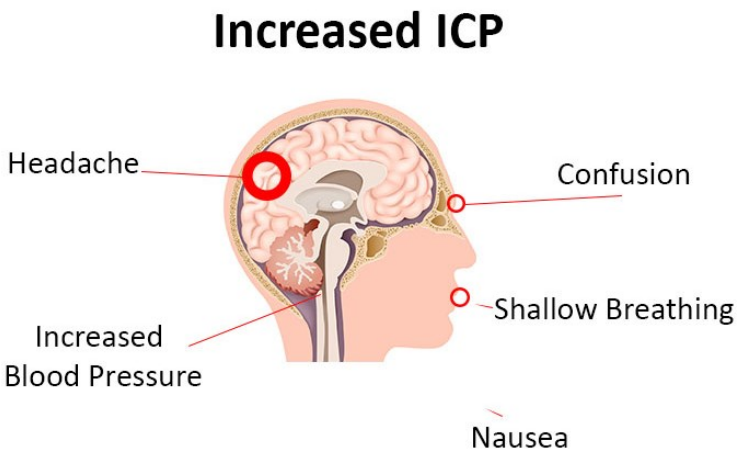

Figure 1. Effects of Elevated Intracranial Pressure

1.3 Research questions and Scope

ICP is one of the common consequences of traumatic conditions and has a profound influence on outcome. There are well established methods for the measurement, continuous monitoring and treatment of raised ICP. However, there is a need to build computer models for investigation of ICP before any invasive procedures are applied. To-date, there is a lot of research on going, on the measurement of ICP in patients with different conditions e.g. ICP due to edema, ICP due to formation of embolus in CSF and ICP due to accidental head injuries. However, there is still one area in this domain, which is lacking enough knowledge, i.e., investigating ICP due to the presence of brain tumor. Keeping this in view, this project has been divided in four phases which clearly achieve the objectives of this project (more to this later). Suffice to say, this study is a study of CSF-brain tissue interaction in which flow of CSF is modeled and its interaction with brain, keeping ICP in view. In same vein continuing earlier argument, a unique situation in the human brain may occur due to the shearing blood flow across the membranes of central nervous system (CNS) in the human body. This is a very significant area to address in the current world. Human brain acts like a sac allowing major nutrients to supply oxygen across brain for normal working. A phenomenon known for decades, i.e. “The blood-brain barrier” could be one parameter to address this area whereas flow of fluids across cerebrospinal (CSF) region could be another. However, it is pivotal to note that there is a close association between the blood brain barrier and

the pressure that collects inside the brain due to fluctuations in either of the two parameters. Therefore, in this phase of report the flow of CSF in special scenarios (e.g. brain tumor) to map accurate pressures for any life-threatening situations have been discussed. To put succinctly, subject to what has been stated above, the fundamental questions which this work would address are enlisted infra:

(i). How brain tumor affects the flow of CSF and eventually increases the intracranial pressure by deforming/compressing the ventricles of brain and parenchyma?

(ii). If it does, how much can that be helpful in standard model improvement where there are CSF pressure (or also the intracranial pressures) correlation studies which suggest specific pressure ranges for Obstructive Hydrocephalus, Edema et cetera?

(iii). How can we calculate and relate ICP non-invasively by using Image-based finite element modeling?

1.4 Objectives of Study

In backdrop of afore-noted questions supra, following objectives can be drawn which this thesis would aim throughout:-

(1) The current project is aimed at developing the correlation between the ICP and tumor.

(2) Ascertaining relationship of pressure in brain with deformation/displacement caused due to external loading.

(3) Relationship of Tumor to the pressure building on the ventricles and then to the surrounding tissues.

(4) Due to the constriction in the ventricles, usually obstruction occurs in the flow of CSF. This will be investigated for elevation or demotion in ICP in response to the varying complexity.

(5) A full volume of brain model will be developed for accurate modeling and calculation of ICP.

(6) CSF in the accurate model will be modeled mechanistically as viscous fluid to demonstrate blockage.

(7) Combining above in a single finite element model containing both fluid and structural interactions.

The aforenoted objectives of this thesis can be crystalized, in pith and substance, into three stages which include the following concise points for ease of reference for the hereunder:-

(a). Relating ICP with CSF flow in brain ventricles and conclusion drawn thereof.

(b). Relating ICP with Stenosis of Cerebral Aqueduct and its effect on ventricular body and on the flow parameters (if any). This point directly relates to demotion or elevation of ICP because stenosis is inter-alia the conditions which ensues this conditions;

(c). Combining above points together-with the including simplistic brain parenchyma and limited layers thereof and devising fluid-structure interaction, and synopsis drawn thereof (keeping ICP in perspective) based on simulation results.

Since we have to model wall stresses and CSF velocity, pressures through the ventricles and their interaction under the influence of ventricular compression/deformation, there is a need to develop a scheme where both effects can be modeled simultaneously. On the conclusive note, this phase will be investigating the role of CSF in maintaining homeostasis— equilibrium of pressure distributions under both normal and cancerous conditions. More importantly, we also aim to study how brain tumor affects the flow profile of CSF that in turn may introduce different physiological complications such as ischemia and stroke which may otherwise be non-existent; how a ballooning tumor may eventually exhaust the tendency of CSF to work as a buffer; and lastly, how CSF correlation studies may help in a clinical setting by improving the diagnostic process— for both pre-tumoral diagnosis and possible tumor onset, post-tumoral resection.

1.5 Thesis outline

This thesis is carefully and meticulously been drafted keeping in view of the audience and readability. Chapters hereinafter propose to demystify the fundamental question raised (hereinabove) in a coherent and logical manner. Chapter 2 and 3 discusses some of the basics of ICP and its relationship with tumor; why a computational model is needed (or in other words why carry out this study at all?); discusses some of the earlier biomechanical modeling on ICP in past, bifurcating problem in both structural and fluid domain; it introduces fluid-structure (FSI) modeling to the reader which has been extensively used in this thesis. Chapter 4 discusses the methodology part. Chapter 5 and 6 presents the results of this thesis followed by chapter 7 which presents a terse, succinct conclusion and synopsis of the entire thesis.

CHAPTER 2—BRAIN ANATOMY AND ICP

This chapter is exclusively dedicated towards establishing a framework biomechanical modeling of ICP in cases of brain tumor. It looks for some of the already established methods and chalks out strategy for this thesis. In view of foregoing, and to facilitate the reader in grasping contents, this chapter is bifurcated into four sections vis-à-vis biomechanical modeling viz., a brief review of anatomy of brain, CFD based modeling of Cerebrospinal fluid (CSF), structural tissue level modeling and fluid-structure modeling (FSI). In addition to aforesaid, it also presents two additional concepts which would greatly clear the picture in terms of context of undertaking this project viz. the formulation of so-called "Monro-Kellie Doctrine" on ICP and a brief review of tumor mechanics.

2.1 Gross Anatomy of Human Brain

Brain is the central organ of not only human body but also of other invertebrates. It plays an important role in every major body. Some of its key functions include processing the sensory information, regulation of blood pressure, maintaining homeostasis, release of hormones et cetera. Brain can be divided into following major regions: The Cerebrum, the Cerebellum, Diencephalon and the brain stem. Cerebrum is the largest part of the brain. It is further subdivided into two hemispheres (left and right). Both hemispheres are separated by the interhemispheric fissure. Cerebrum contains the cerebral cortex and many subcortical structures and substructures including hippocampus, Basal ganglia and olfactory bulb [5].

Furthermore, each cerebral hemisphere is partitioned into different regions or lobes based on the functionality of each region (the picture is taken, with approval, from [6]). These lobes are enumerated herein below [6]:

(i). **Frontal Lobe:** The Frontal lobe is an important part of the brain which conducts various cognitive control mechanisms in the body. The mechanisms inter alia include control of voluntary motor functions, expression of emotional setting, memory, decision-making, sexual behaviors, smell reception etc.

(ii). **Temporal Lobe:** The Temporal lobe is involved in performing and actualizing the functions of olfactory (smelling) and auditory (hearing) sensations and, also plays a

pivotal role in the memory aspect. It is isolated and separated from the cerebrum via **"lateral fissure"**.

(iii). **Parietal Lobe:** The Parietal lobe rests above the temporal lobe and is separated from the frontal lobe via "**central sulcus"**. Parietal lobe is the epicenter for receiving and processing most of the sensory data such as that of obtained through touch, smell, temperature etc.

(iv). **Occipital Lobe:** The Occipital lobe is the center of visual processing and is not separated from other lobes distinctly. It sits in the rearmost portion of the skull and performs the integration of visual data obtained through eye (figure 2[2] taken from Seeley's essential on anatomy [6]).

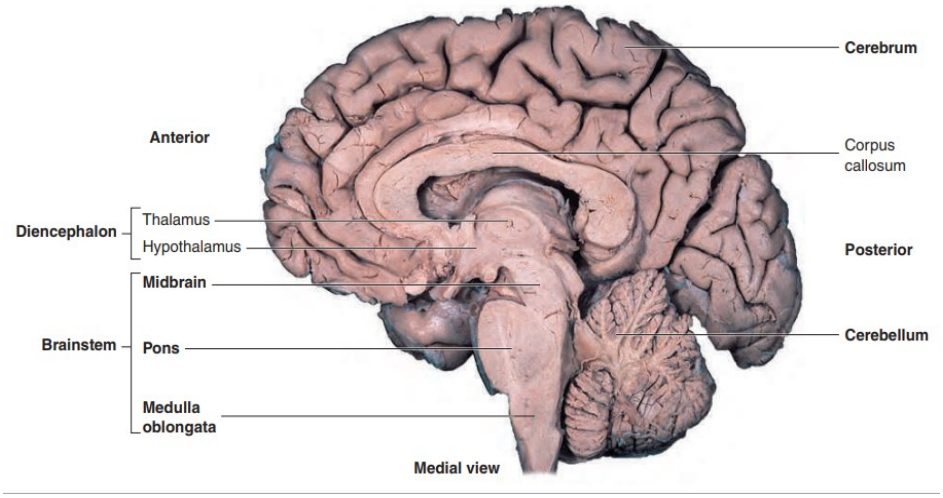

Figure 2. Side view of brain showing different structures of brain

[2] Picture taken from [6]

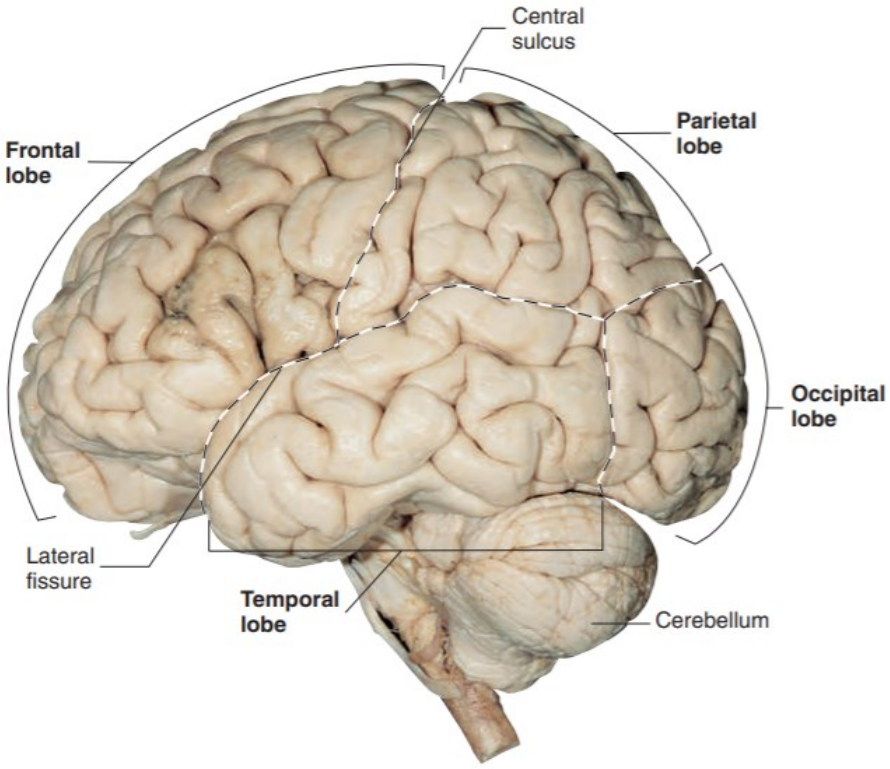

Figure 3: Topographical representation of Brain

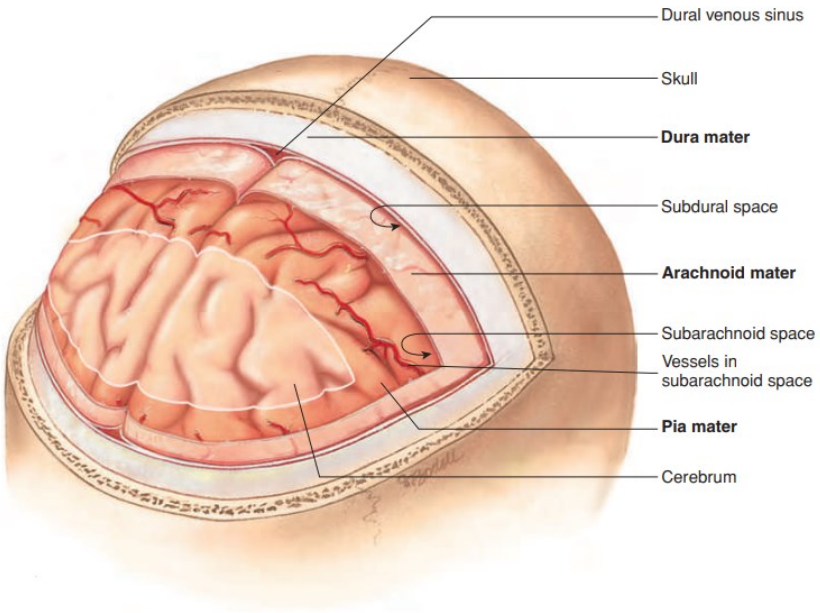

Figure 4: Anterior Superior view of head showing Meninges Layer

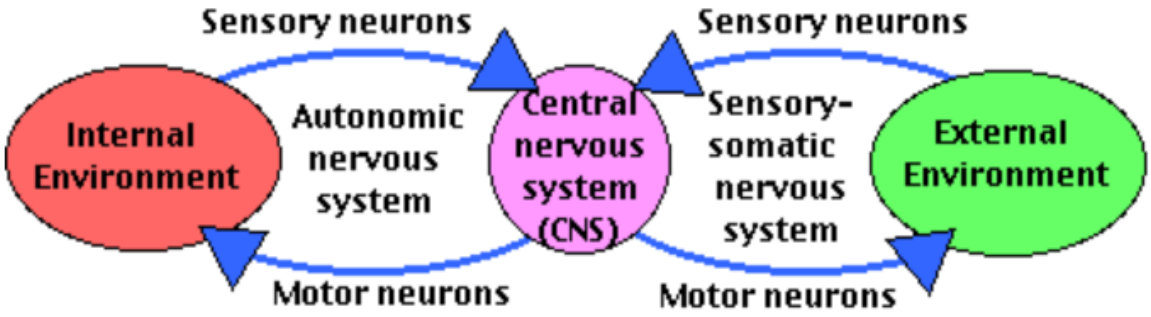

Figure 5: Pictorial representation of entire Nervous system working

The Human brain is connected not only to itself but to the entire body via two connection systems viz. Central Nervous System **(hereinafter referred to as CNS)** and Peripheral Nervous System **(hereinafter referred to as PNS) (and collectively called as Nervous system)** [5-6]. The CNS is composed of the Brain and the Spinal cord. Entire processed information travels to and fro, through the spinal cord, from the Brain to the periphery. Hence the Spinal cord is the junction between the ***'isolated'*** brain and lower torso. The CNS and PNS interact continuously in a dynamic and synchronized manner forming the *Nervous System*. As with the case of Skull being the protective layer for the brain, Spinal cord, too, is protected via vertebral column. In addition, brain and spinal cord are both encapsulated within Meninges [6]. Meninges is a set of three membranes which covers the brain and the spinal cord in invertebrates [5-7]. In the case of humans, it is composed of following layers viz. Dura mater, Arachnoid mater and Pia mater (picture above, figure 3 taken with approval from [6]). The intracranial fluid, also called the Cerebrospinal fluid **(hereinafter referred to as CSF)**, is present within the spaces of these layers which is also sometimes referred to as Subarachnoid space. The main purpose of these layers, as with the case of skull, is to protect the brain from any unwarranted injury. The PNS is further divided into three parts viz. Somatic, Autonomic and Enteric nervous systems[3] (figure 4). The Somatic nervous system **(SNS)** performs the voluntary movements of body via skeletal muscles [5]. Thus, all movements are associated to and linked with SNS. The Autonomic nervous system **(ANS)** is related with the functioning of internal organs (smooth muscles and glands). It may aptly be called

[3] Picture (figure 5) taken from <https://bio.libretexts.org/Bookshelves/Introductory_and_General_Biology/Book%3A_Biology_(Kimball)/Unit_15%3A_The_Anatomy_and_Physiolobgy_of_Animals/15.08%3A_Nervous_System/15.8D%3A_The_Peripheral_Nervous_System> accessed 14th August, 2019

as a control system that acts involuntarily and regulates the functions of body, inter alia, heart rate, urination, digestion, rate of respiration et cetera. The Enteric nervous system **(ENS)** can be thought of as a localized or intrinsic nervous system that acts at a certain level on its own, usually found in gastrointestinal tract [5]. It contains millions of neural circuits which integrate all the information (about the condition of gastrointestinal tract) and subsequently controls the gut movement (based on the processed information).

Apart from the topographical classification supra, the CNS, in terms of substance (matter), can be subdivided into two components viz. Gray Matter **(hereinafter referred to as GM)** and White Matter **(hereinafter referred to as WM)**. The GM is the outer layer of the brain and consists of neuronal cell bodies, dendrites and axon terminals (having the synapses of neurons). Whereas, the WM consists of axonal terminals which interconnect different regions of Gray Matter. The GM is found on the outermost layer of the brain i.e. on the cortical surface, while the WM is found below the cortical surface (as shown in figure 5) [5]. There are also some subcortical nuclei, also called the **Basal Ganglia**, situated in the forebrain and at the top of the brain. These *inter alia* include Caudate nucleus, Pallidum, Putamen et cetera. Primary functions of Basal Ganglia include, amongst other, controlling voluntary movements, cognition, learning, emotions et cetera [7].

Moreover, the brain is submerged in the CSF which provides the cushioning effect and also behaves as a shock absorber; it protects from any unwarranted injury. CSF is a dense viscous fluid which is produced in the **'Choroid Plexus'** found inside the walls of Ventricles. Ventricles are cavities or sac like structures and function as containers for CSF. There are two lateral ventricles (left and right) on both sides of cerebral cortex [5-6]. Lateral ventricles are connected to each other via **Interventricular Foramina** which is the junction from which CSF passes into the **'Third Ventricle'**. The CSF from the third ventricle extends into **Aqueduct of Sylvius** (or cerebral aqueduct) which then ends into the **'Fourth Ventricle'** thereafter CSF circulates both in the Spinal cord and around the Subarachnoid space (see figure 6[4]).

[4] Figure taken from Seeley's essential [6]

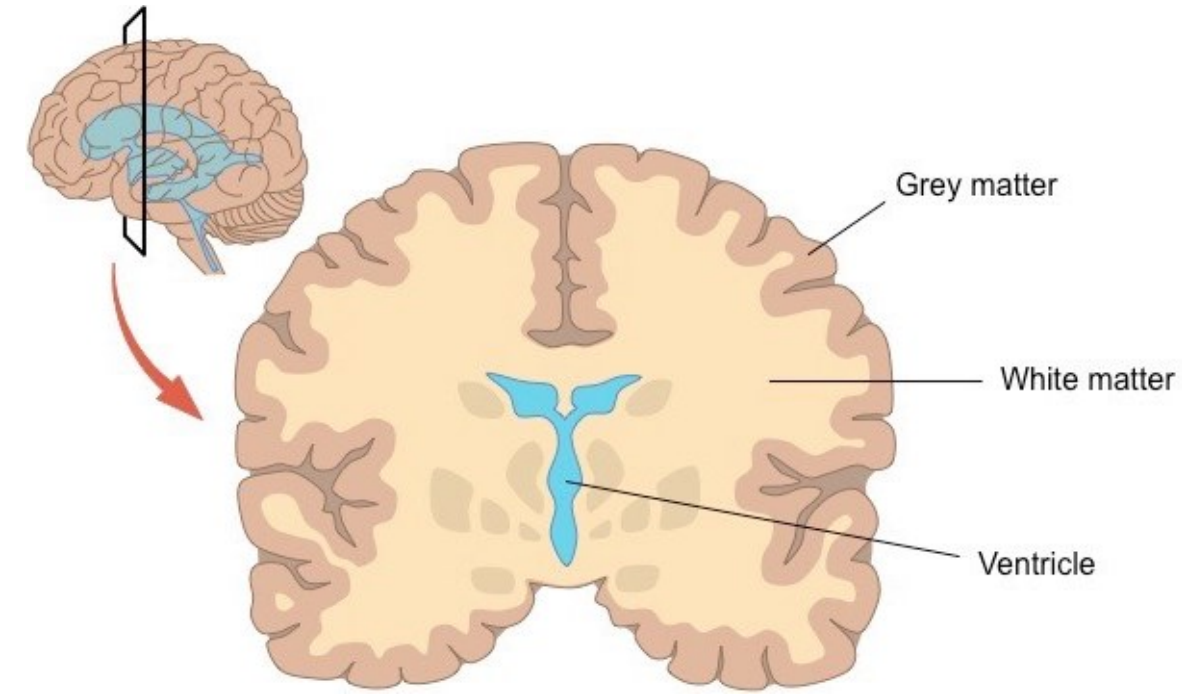

Figure 6: Cross-section of Brain showing Gray and White Matter

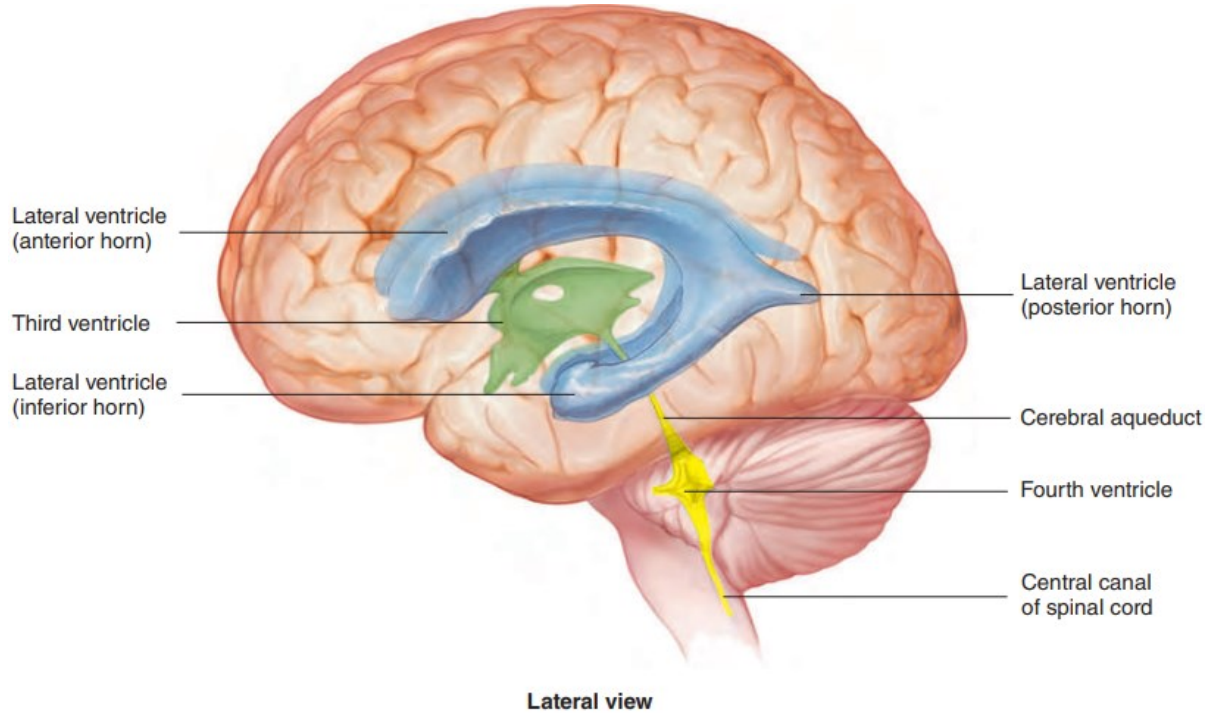

Figure 7. Ventricles of Brain Shown from Lateral view

At normal conditions, the production rate of CSF generally approximate to around **0.3 millimeters/minutes (or 500 ml/day)** [5]. Any disorders in production or reabsorption of CSF produces grave clinical dangers. One of the dangers associated with the problems in either absorption or production of CSF is **'Hydrocephalus'**. Hydrocephalus refers to the fluid buildup in the ventricles of brain which creates an increased hydrostatic pressure (pressure due to the fluid) gradient in surroundings and hence constricts fluid motion [1][5][6][8].

The blood supply to the brain is through the following sources: from carotid arteries (left and right), vertebral arteries (left and right) and capillaries emanating thereon [6]. The blood leading towards brain (in arteries and capillaries) apply pressure inside the walls of arteries. This pressure is called arterial blood pressure; and usually by way of average, in a single cardiac cycle, it is also termed as the Mean Arterial pressure **(**hereinafter referred to as **MAP)**. Similarly, the net pressure with which the blood forces into the brain is called the Cerebral Perfusion pressure (hereinafter referred to as **CPP)**. Whereas, the ICP is defined as the pressure inside the cranium and is related to both the MAP and CPP through the following equation [9-11]:

$$\mathbf{CPP = MAP - ICP} \tag{2.1}$$

The nature of equation (2.1) is dynamic and is deterministic. The ICP changes with respect to the changes in arterial pressure (due to arterial pulsation), sneezing or coughing [9]. Likewise, the volume of CSF change with circulation, absorption, creation and reabsorption over a period of time and thus change ICP as well [9-11]. Suffice to say, the nature of ICP is time dependent; this equation has to be fitted in overall framework (more to this later).

As a result of what has been discussed above, the equation (2.1) in general cannot be used because the variables therein change with respect to time and it would be tedious to calculate them independently. We need ergo a different mechanism to study the relationship of ICP through which we can calculate the same.

2.2 Monro-Kellie Doctrine and ICP

Alexander Monro, more than two centuries ago, studied the blood flow in the intracranial compartment, and through various calculations concluded, by way of hypothesis, that the blood circulating inside the skull was constant at all the times. This proposition/hypothesis was also supported, through series of experiments, by George Kellie in 1824. This later became **'Monro-**

Kellie Hypothesis' and, after two centuries later is still adopted and carefully considered in neurosurgery [12]. The Monro-Kellie Hypothesis states that the total sum of volumes of intracranial compartment is constant, i.e. the sum of volumes of brain, CSF and Blood remains the same. Thus, there is no net change in the intracranial volumes at any given instant. If, by way of any disorder, the volume of any intracranial constituent changes (either increases or decreases) then the other intracranial constituents must compensate for the change so as to ensure the net change to zero. This compensation comes at a cost: if the volume of the one constituent increases then the pressure of other constituents must necessarily increase (in order for their volume to decrease) and is reflected hereinbelow by way of graph (taken with approval from [12]):

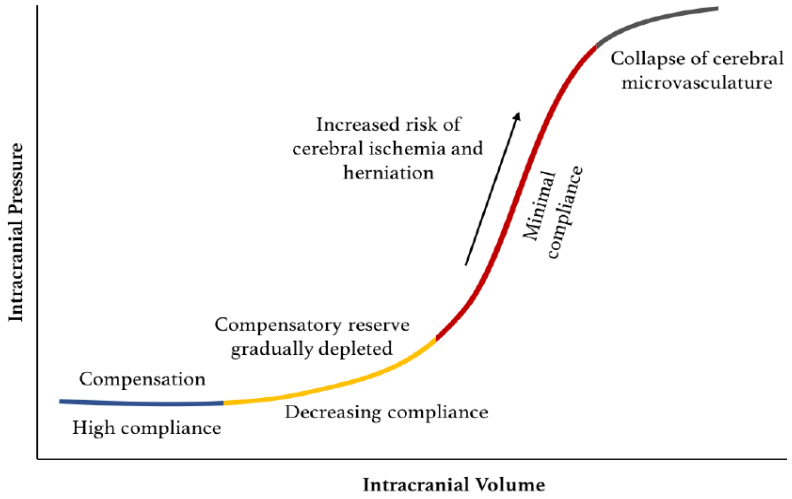

Figure 8. Relationship between Intracranial Pressure and Intracranial Volume.

The graph supra paints the following picture which can be paraphrased as:

(i). Brain is linearly elastic (or more precisely viscoelastic) in nature and therefore can deform elastically (or Visco-elastically) to compensate for loading and pressure distributions, also called intracranial compliance.

(ii). Initially, the compliance is higher but as pressure increases, compliance decreases due to increasing forces.

(iii). A point comes when the pressure increases beyond limits resulting in exhaustion of compliance mechanism; and thereafter no volume increases significantly. This point is where severe herniation can take place; brain structures can deform plastically (permanent); constriction of veins can occur causing hemorrhage et cetera.

(iv). This consistent pressure rise in ICP needs significant monitoring especially when the ICP has gone beyond compliance limits.

2.3 ICP and Brain Tumor Mechanics

Brain tumor is a special condition in which brain cells grow and multiply abnormally. This amplification in growth results in an increase in mass content of brain. The principle of Monro-Kellie holds that intracranial contents remain same (as discussed above). In this case, the intracranial volume of brain tissue increases, whilst maintaining an equal decrease in volume of CSF and blood so as to maintain dynamic relationship (see figure 8 for volume pressure relationship).

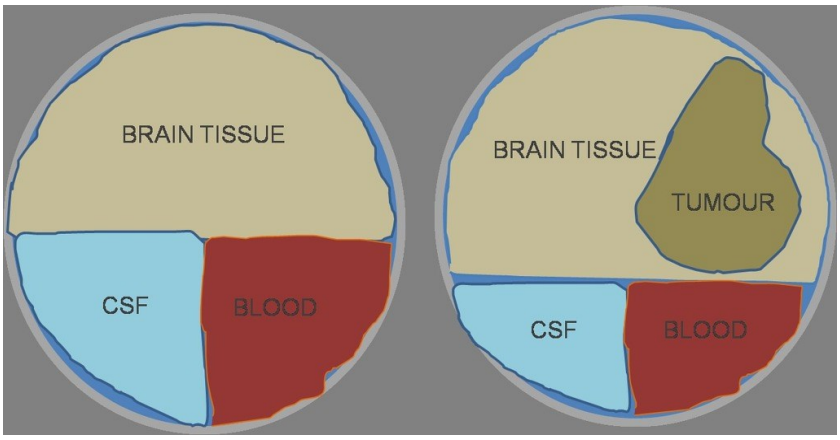

Figure 9. Intracranial constituents and Brain Tumor interplay

Thus, as evident from the pictorial representation above (figure 8), it can be safely and confidently be concluded that: (1) Brain tumor increases mass content of the brain; (2) that this increase ought to be offset by either proportional or disproportional decrease in either one or both constituents (as the case may be); and (3) that because volume has to be offset therefore pressure must evidently increase so as to manage or make that corresponding change in volumes thereof.

2.4 Monitoring of ICP—Why a computational model

ICP is measured in mmHg (millimeters of Mercury) units. The measurement and monitoring of ICP is difficult and involves complex procedures. In followings paragraphs, a brief review on available techniques to measure and monitor ICP is presented; and which will further give a persuasive argument for developing a computational model of ICP, by which doctors and other relevant people can calculate the ICP non-invasively. Firstly, according to American Brain trauma foundation [13], monitoring of ICP indicated in all cases a *Glasgow Comma Scale*

(hereinafter referred to as "GCS") between 3-8 together with an abnormal Computed Tomography **("CT")** scan. GCS underlines a reliable and objective way to monitor the state of consciousness of a person. It is helpful, indeed, when using in cases of traumatic brain injuries and also for tumor patients. However, it does not provide the complete picture, and only suggests the awareness of patient under certain neurological conditions. It does not tell us anything about the level of ICP *per se*. Whereas, on a broader scale, there are two methods for measuring and continuous monitoring of ICP: Invasive and non-Invasive methods. Let us first discuss very briefly about some invasive methods. There are several invasive methods for measurement ICP. These depend upon the anatomical locations from where measurement is done. Two of the popular methods are detailed hereinbelow: **External Ventricular Drainage (EVD)** is an invasive monitoring of ICP, where a catheter is placed in the ventricles through a hole. The value so recorded is also sometimes called gold standard. It is also used in draining the CSF to relieve high pressure [14-17]. The method is associated with few risks like hemorrhagic and infectious complications. **Micro-transducer ICP monitoring Devices** are a group of devices which can be divided into fiber optics, strain gauge devices and pneumatic sensors [14]. However, these devices do not provide the necessary accuracy for routine use. There are various methods to measure ICP non-invasively. **Transcranial Doppler Ultrasonography (TCD)** applies ultrasound to measure the blood flow velocity. The difference between systolic flow velocity and diastolic flow velocity divided by the mean flow velocity gives pulsating index PI (see equation 2.2). The PI correlates with measured ICP (invasively) as outlined by [11][14].

$$\mathrm{PI} = \frac{\textbf{systolic flow velocity} - \textbf{diastolic flow velocity}}{\textbf{mean flow velocity}} \qquad \textbf{(2.2)}$$

Recently, **Magnetic Resonance Imaging (MRI) and Computer Tomography (CT)** are used to investigate the possibility of measuring ICP non-invasively. The technique relies upon a finding set of parameters from a motion sensitive MRI which include arterial, venous and CSF flow in and out of the cranial vault during a cardiac cycle [18]. The volume change is calculated from net CSF and blood flows (volumetric) and then CSF velocity is calculated which is further used to infer/estimate the pressure. An **elastance index** is calculated which is the ratio of pressure to volume change and Alperin et.al found that it correlates with the measured ICP well (R^2=0.965; P<0.005) [18]. Similar studies are also reported for CT scans. In purview of the aforenoted discussion, it can be deduced, from the outset, that there are impediments in monitoring ICP

continuously especially when using invasive methods (such as External Ventricular Drainage) which involve risks of hemorrhagic and infectious complications.

Fortunately, with the advent of Image based modeling and finite element methods, the need for computer-based models and non-invasive methods have increased. The computational power has increased and, complex and intricate systems can easily be modelled. For example, there are various models available for heart which are used to gain prior knowledge before operating on a patient. Having to use computational models gives us many benefits: first the risks are reduced compared to situations where invasive procedures are applied. Second, models help us in gaining knowledge and valuable insight into the behavior of the phenomenon. Third, models are designed to introduce complexities which are otherwise difficult to comprehend. There is also another compelling argument for opting for devising a model to study it. Every year many people die because of tumor due to late diagnosis **(in 3rd stage)** after which cure is of no worth (usually). The interdependence of ICP and tumor, if explored in quantitative sense, will help doctors to diagnose it at an early stage; and naturally treatment becomes easier when tumor has not spread (or has not metamorphosed into malignant). It is against this backdrop that this thesis aims to establish a functional correspondence between tumor and ICP which will help doctors to take informed decisions.

2.5 Strategy for developing Computational Model

As discussed in preceding paragraphs, a computational model is needed to study the biomechanical relationship between ICP and Brain tumor so as to improve prognostic potential of early detection of tumor. The computational model in this case has primarily two parts: Segmenting the tumor and brain layers (because brain is inhomogeneous and has different properties in different directions and thus analyses need to be done accordingly); and second, we need to apply FEM equations/analyses to find the constitutive relationships between ICP and tumor. In pith and substance, modeling of ICP has three broad dimensions which are represented in fig. Also, the underlying FSI principle which dictates the entire project scheme is also shown via pictorial representation.

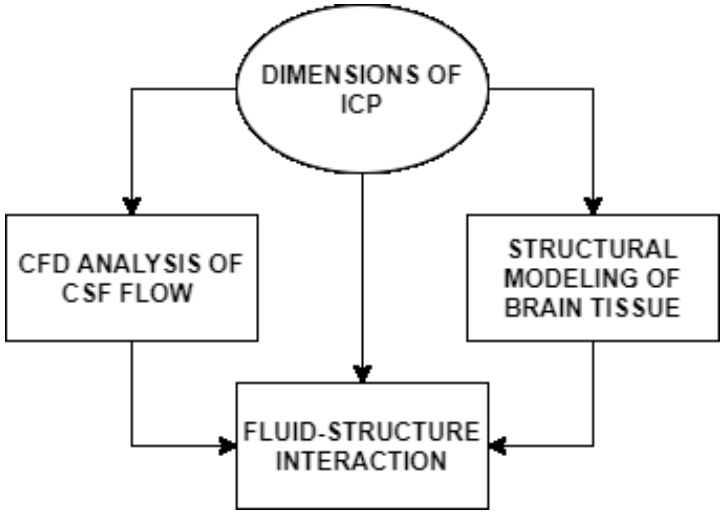

Figure 10. Dimensions of ICP

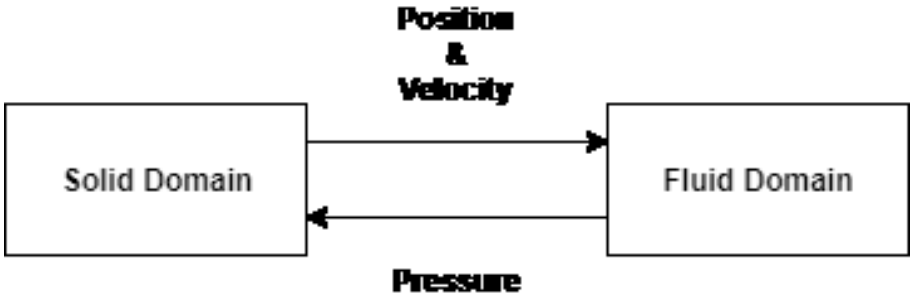

Figure 11. FSI Principle

Hereinafter the thesis would carry and revolve the dimensions of ICP from three broad perspectives. First, the Computational fluid dynamics (CFD) analysis of CSF flow in brain ventricles and overall; second perspective pertains to the structural (tissue-level) modeling of brain and ascertaining the material properties of brain tissue; third, this thesis will broadly and mainly will be the conglomeration (or combination) of both the fluid and structural interaction (hence I would only restrict myself to FSI, and would not indulge in mentioning other relatable factors to ICP such as blood pressure etc. Some clarifications regarding dataset used in this thesis would come later in their appropriate sections). The FSI principle is supplied hereinabove in figure 10. It encapsulates transfer of data of forces and velocity (or displacements) from both sides and is either one-way or two-way. Basic difference between the two is that one-way FSI is unidirectional and only transfers one side of data. Two-way FSI paints a complete picture and interaction inter se the solvers.

CHAPTER 3—LITERATURE REVIEW

In order to develop the computational model, we need to first analyze the literature available on it. The Literature review has been distributed into two parts. This chapter effectively deals with the presentation of techniques for segmentation of Tumor and Brain layers. It is also dedicated towards the review of biomechanical modeling in past on the problem of relating ICP and analyzing it with respect to CSF flow and its interaction with brain parenchyma and different layers. Following block diagram (figure 12) is provided which chalks out in simplest terms how I would proceed for the materials and methods section.

3.1 Segmentation of Tumor and Brain layers

Manual Segmentation of tumor and different brain layers is, in general, a very complicated and tedious task for a Radiologist. In manual segmentation, radiologist uses hand to segment the boundaries and label the image. Since medical images consist of many slices which can range to hundreds, therefore, manual segmentation becomes tedious and time-consuming task as the radiologist must go through each slice individually [19]. Manual methods are also prone to human errors due to variability in the expertise of operators and physicians. However, manual techniques are still being used to define the ground truth for automated techniques and mapping of human brain [20-21]. Therefore, due to human error and time consumption it is infeasible for physician to manually segment and assess brain tumors given a large dataset. At the same time, segmenting various brain layers such as White matter (WM), Gray Matter (GM), Ventricles etc. is also a hefty task which cannot be done in a clinical setting by a Radiologist. Hence, radiologist often resort to automated methods.

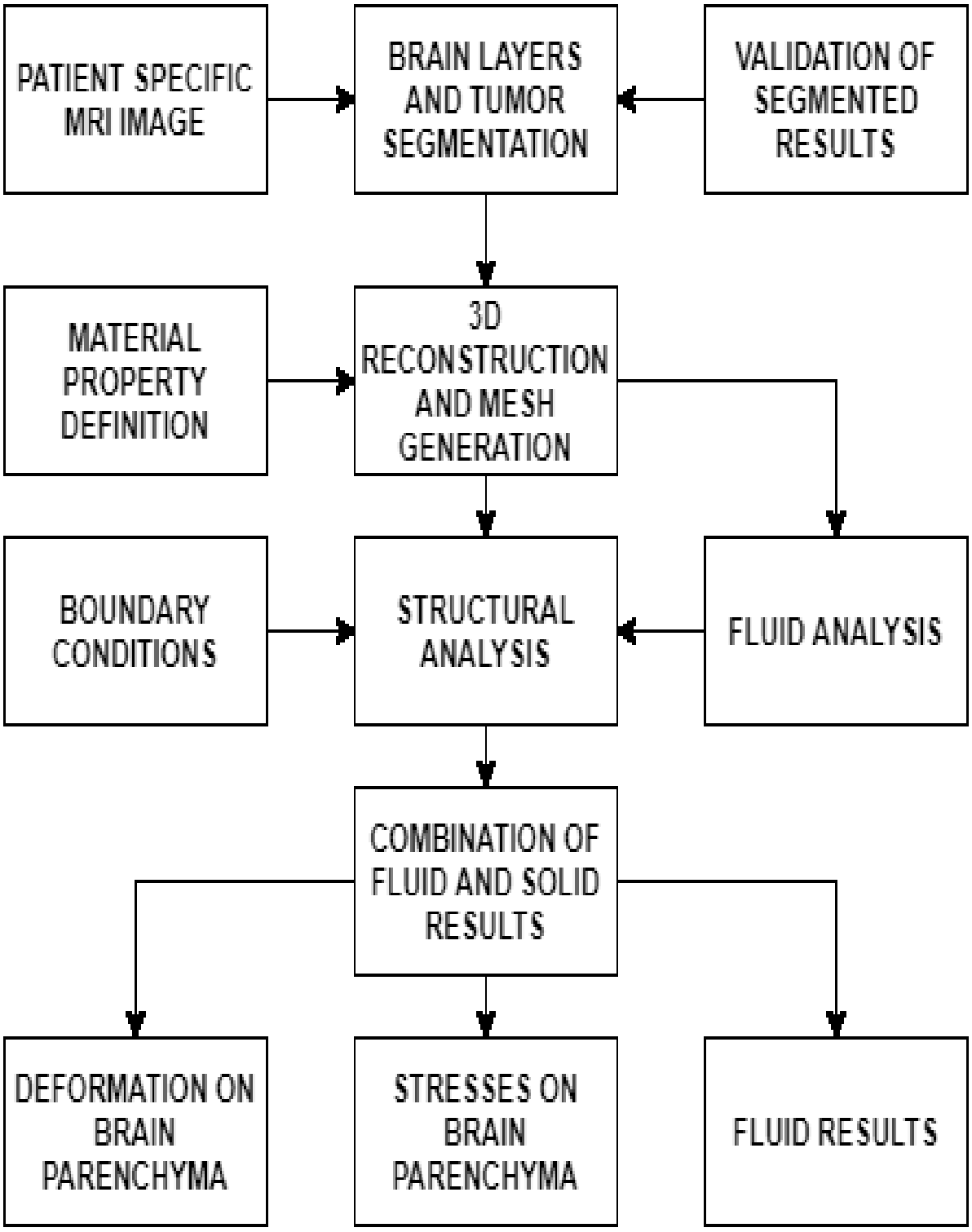

Figure 12. Block Diagram depicting proposed methodology

3.1.1. Intensity-Based Methods

Automated methods use advance computer vision techniques and algorithms to detect and segment brain tumor. Intensity based techniques are the most common and easy to implement. The intensity of each pixel/voxel in medical images is used to segment different components. In brain MRI images usually gray matter (GM), white matter (WM) and CSF are distinguished using such techniques. Thresholding methods are common amongst intensity-based techniques. Thresholding techniques use intensity histogram and then differentiate gray levels based on their intensities. The common thresholding [19] methods are Otsu's method, local thresholding, global thresholding, multi-level thresholding etc. For instance, global thresholding is defined as:

$$\mathbf{I(i,j)} = \begin{cases} \mathbf{1}, \boldsymbol{if}\ \boldsymbol{I(i,j)} > \mathbf{T} \\ \mathbf{0}, \boldsymbol{if}\ \boldsymbol{(I,j)} \leq \mathbf{T} \end{cases} \quad \textbf{(3.1)}$$

where i, j are pixel coordinates, I (i, j) is the segmented image and T is the threshold value.

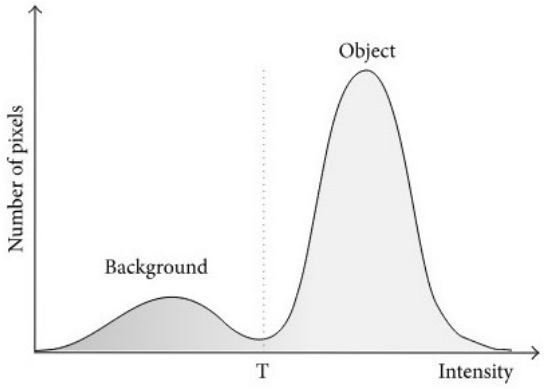

Figure 13. Image Intensity based operation

Thresholding methods are computationally fast but are sensitive to noise and intensity variation and they also do not consider the neighborhood information. T. Weglinski et al. [23] proposed a region growing method to segment brain tumor from MRI images. Region growing is a technique for extracting a connected region of the image which consists of groups of pixels/voxels with similar intensities. In this method starting point is selected manually or in an automated way and then its neighbor pixels are examined. The region grows so long the neighboring pixels fulfill the criteria. Whereas, thresholding techniques still utilize some prior preprocessing steps to segment brain tissues and skull.

3.1.2. Unsupervised Classification-Based Methods

Classification methods use data with known labels to partition image feature space. Image features are typically intensity values but can be also related to texture or other image properties. Classification methods can be both supervised and unsupervised. **K-nearest-neighbor** (*k*NN) is a common classifier, where the pixel/voxel is classified according to the majority vote of the closest training data. The *k*NN classifier is considered a nonparametric classifier because it makes no underlying assumption about the statistical structure of the data. Warfield et al. [24] proposed the use kNN classification method to segment tumor from brain MRI images. In another paper, P. Dhanalakshmi et al [25] described yet another technique for segmentation of tumor from brain MRI images. The authors have used K-means clustering in their piece of work. The proposed method for segmentation is as follows: prepossessing is done with bias field correction, intensity normalization, median filter for noise removal, and image sharpening. Image is segmented using K-means clustering method. The method is based on unsupervised learning. It first assigns number of clusters, then randomly initializes cluster centers, feature vector (image data) are group into k clusters depending upon the distance from the cluster centers. The algorithm continues until convergence. The resultant image is a labeled image which has clusters of same intensity. However, the major drawback of this method, as with those methods similar to this one, is that it is sensitive to noise. Ahmed N et al [26] proposed yet another segmentation technique based upon modified fuzzy C means clustering. In practice, intensities of pixels are inhomogeneous in MRI image. This inhomogeneity is introduced partly due to the scanning capacity and limitations of system per se. Therefore, the result of segmentation is poor. The authors have proposed a technique based upon an objective function which compensates for intensities inhomogeneities thereby reducing the chance of assigning labels to spurious pixels in its vicinities—by having a neighborhood regularize function. Classical fuzzy C means function is given as:

$$\boldsymbol{J = \sum_{i=1}^{c} \sum_{k=1}^{N} (uik)^{p} \, \|x(k) - vi\|} \qquad \textbf{(3.2)}$$

In equation (above) $\boldsymbol{uik}$ is the cluster component, and p (an exponent) is the fuzziness index. In purview of the defined equation, the authors have proposed a modified form which also considers the neighborhood of voxel/pixel. The neighborhood acts as a regularizer and biases the solution towards the piecewise homogenous labelling. Likewise, the method is very useful when we have a different bias field issues and the results reported by authors are very significant inasmuch as to the case of intensity inhomogeneities and segmenting gray and white matter from

images is concerned. Whereas, Karim Kalti et al [27] proposed another segmentation technique based on Gaussian mixture models coupled with fuzzy-C means. The authors propose a method based on variant of both expectation maximization algorithm and fuzzy C means, to address the issue of noise sensitivity. They opted two features for the characterization of the pixels of image: First feature is the value which describes the properties of a pixel. Second feature looks for the neighborhood of the pixel. The method relies upon the adaptive distance metric which describes either of the features according to spatial resolution of the image. The method uses a threshold value which is empirically determined. However, the main drawback of this method is that the performance of the segmentation is mainly dependent upon the threshold chosen and it varies according to image data.

3.1.3. Level Set and Active Contour Based Methods

Ali M. Hasan et al [28] proposed a segmentation technique based on Active contour model the authors have proposed an automated segmentation technique that can segment tumor effectively from MRI scans. The method proposed by the authors is as follows: firstly, preprocessing is done on the image to clean stray pixels and remove noise. Then, gray-level co-occurrence matrix and Analysis of Variance **("ANOVA")** is applied for feature extraction. A multi-layer neural network is adopted as a classifier and 3D bounding box based on genetic algorithm is used to find the location of tumor in the MRI slices. Lastly, 3D active contour without edge is applied to segment tumor. The initial contour is evolved using level set method; and the stopping condition is the minimization of Mumford-Shah energy function:

$$\boldsymbol{F^{MS}(u,c) = \int_{\Omega}(u-1)^2 dxdydz + u \int_{\overline{C}}|\nabla u|^2 dxdydz + \vartheta|C|} \quad \textbf{(3.3)}$$

Where u approaches the Image function I, and Ω is the image domain of connected components, C is the boundary of the contour, c1 and c2 are the values inside and outside the contour C and ϑ is a constant. While u is defined as:

$$\boldsymbol{u(x,y) = \begin{cases} c1 \text{ where } x,y \text{ and } z \text{ are inside } C \\ c2 \text{ where } x,y \text{ and } z \text{ are outside } C \end{cases}} \quad \textbf{(3.4)}$$

The Chan-Vese model imposes a penalty on the Mumford-Shah function to minimize the same for convergence. The accuracy obtained was 89% with a tolerance of 4% compared with manual process. C. Baillard et al [29] describes a strategy for the segmentation of brain MRI (Volume) Images which incorporates processes of Segmentation and Registration in 3D. First, the

Segmentation process includes the usage of level set method. Level set methods are used to define the shape of the image (through segmentation) by first partitioning the image (or topology) using different planes. Thereafter, the authors define a Curve S(t) as:

$$\boldsymbol{S(t)} = \begin{cases} \boldsymbol{X} \in \boldsymbol{R} | ¥(\boldsymbol{x}, \boldsymbol{y}) = \boldsymbol{0} \\ ¥(\boldsymbol{x}, \boldsymbol{y}) = \boldsymbol{d} \end{cases} \quad \textbf{(3.5)}$$

Where ¥ (x, y) gives the surface by the given distance d. The level with which the function evolves over time is given by:

$$\frac{\boldsymbol{d¥}}{\boldsymbol{dt}} + \boldsymbol{F}|\boldsymbol{\nabla ¥}| = \boldsymbol{0} \quad \textbf{(3.6)}$$

Where F is the scalar velocity and depending upon the local properties such as the curvature of the curve. The Surface ¥ deforms iteratively through the velocity function F and the S(t) of the surface is given by the function equation (above). Lastly, the curvature of the curve is given by taking the divergence of the equation:

$$\boldsymbol{\varphi} = \boldsymbol{div}\left(\frac{\boldsymbol{\nabla ¥}}{|\boldsymbol{\nabla ¥}|}\right) \quad \textbf{(3.7)}$$

After the segmentation process, the authors use a multi-resolution nonlinear registration-based method to register the segmented output to an atlas.

3.1.4. Deep Learning-Based Methods

It goes without saying that Convolutional Neural Networks **(hereinafter referred to as "CNN")** have dominated the present discourse in Medical Imaging for quite some time for atleast two reasons: First, the availability of large data has made easier to train complex models thereby achieving exceptional performance relative to other supervised or clustering techniques; and second, they are mostly easy to implement particularly given the fact that most models are pretrained or there architectures are easily available. In pith and substance, these use the concept of neural networks and their associated learning techniques to automatically segment the Region of interest **("ROI")**. However, a partial handicap towards implementing them is that these require high performance computing facilities such as Graphical processing units **("GPU")** for parallelizing the processes, and a labelled image is required (by radiologist) to learn the features. In a paper authored by Pereira et al [30], authors have proposed a segmentation technique of gliomas from MRI images of brain. The method proposed a CNN—an automatic segmentation method based on workings observed from neurons of human brain. The proposed method is as follows: firstly, image is preprocessed using bias field correction and intensity normalization. After

that, the training on dataset is done by using samples of both high gradient gliomas **("HGG")** and low gradient gliomas **("LGG")**. The Convolutional layer uses 3x3 kernels. The authors have used BRATS 2013 dataset to validate their results and obtained the dice similarity coefficient of 0.88, 0.83 and 0.77 of complete, core and enhancing tumors. In another paper, Havaei et al [31] proposed yet another segmentation technique which uses framework of Deep Neural Networks **("DNN")**. Results reported on the 2013 BRATS test dataset reveal that architecture improves over the currently published state-of-the-art while being over 30 times faster. In a similar paper, Alexandre et al. [32] has proposed the use of DNN in a different manner. They have used the dataset provided for MICCAI 2012 challenge on multi-atlas labeling, which consists of 35 manually segmented MR images of the brain. Their technique achieved mean dice coefficient of 0.725 and error rate of 0.163. Authors also claim to be the first one tackle the anatomical segmentation of the whole brain using deep neural networks.

Limitations or drawbacks of aforementioned methods:

One of the major limitation of aforementioned methods, keeping the particular aims of thesis, is that since I want to have an accurate anatomical representation (or as far as possible) of brain parenchyma, and since either manual or deep learning based methods need existing labels which in a clinical setting is nearly non-existent ergo I need to go for another method (such as atlas-based registration method defined hereinbelow) from which two aims can be achieved: (1) the problem of validation and (2) finding, as far as possible, accurate representation of brain parenchyma.

3.1.5. Atlas Based Registration Methods

In addition to abovementioned methods, there are some other segmentation methods which cater for the neighborhood information and geometrical constraints and are usually defined through a set of structures or collectively called as atlas. This information (of all anatomical structures) are incorporated in an atlas with correct labelling of brain anatomy. Thus, for example, the occipital lobe and parietal lobe usually cannot be segmented through conventional means but if one was to compare a subject volume with that of a standard brain atlas, one can easily annotate the given volume based on the standard atlas. Hence, given an MRI Volume, one can easily segment the image, by mapping the axes of coordinate space into that of an atlas in an anatomically correct way. This process is usually referred to as Registration [33]. Since a one-to-one mapping

of coordinate spaces is involved in registration and because the anatomical structures (Input MRI Volume) can vary subject to subject, hence the process of registration must be a deformable one, i.e. the given subject must be mapped on the atlas in a non-rigid fashion to cater to the intricate complexities of the intracranial anatomical structures. Let's suppose we have two 3D Scalar (Volume) Images, A: R^3->R and B: R^3->R. We also assume that each voxel correspond in A has an equivalent voxel in B. For this correspondence, we need a **"Transformation Matrix"** $\boldsymbol{F}$ [33], which transforms the coordinate space of A to B. For a coordinate point in A (x, y, z), the corresponding point in B shall be given by F (x, y, z). Thus, for any location *I*, we can write the correspondence between the Atlas (say G) and the given image as:

$$\boldsymbol{I \rightarrow G(F(x, y, z))} \quad \textbf{(3.8)}$$

Bruce Fischl [34] gives a software platform which performs the structural, anatomical and functional processing of MRI images. The software has the capability to perform volume registration between the given volume and a standard atlas of brain. All visible anatomical structures such as Hippocampus, WM, brain stem etc. can be easily segmented using the software. The software also can also reconstruct the cortical surface models of the cerebral cortex (mostly used in FMRI studies). The Cortical parcellation (annotating the image) is done through by using different brain atlases mostly used are Desikan-Killiany Atlas and the Destrieux Atlas given respectively by [35-36]. Hence for segmentation of brain parenchyma layers FreeSurfer is used.

3.2. Biomechanical modeling in Past

This part effectively deals with the biomechanical modeling of ICP in past from two perspectives, i.e., CFD analysis of CSF and tissue level modeling of brain and *inter se* interaction. In this part, I would analyze the aforesaid sections, dwelling deep into their multifarious concepts related to my part of thesis, and would try not to indulge in repetition (Also, I view this part as most important part of this thesis so hereinafter a detailed and multi-dimensional approach would be taken to make the reader understand where the scientific knowledge stand at this juncture on the title of this thesis).

3.2.1. Computational Fluid Dynamics of CSF

In recent decades, numerical methods along with computer simulations are commonly being used to discretize real life scenarios such as blood flow in arteries, cardiac muscle modelling

et cetera. In research areas containing biomedical applications such techniques are useful because they are non-invasive and allow clinicians to take informed decisions prior to any sensitive invasive procedure. Computational fluid dynamics (CFD) has been widely used to model CSF flow. Analysis of CSF behavior and properties such as velocity profile and pressure drop through ventricles under influence of any pathology allow the clinicians to differentiate between normal and abnormal cases. CSF modelling has been of great interest by researchers from across the globe. For instance, one of the proposed model [37] consists of a simple cylinder model to study the flow of CSF through of cerebral aqueduct. Ibid study suggests that pressure difference of atleast 1.1 Pa is required to drive the CSF from cerebral aqueduct. Another study [38] also proposed two models, cylindrical rigid wall model and elastic wall model segmented from MRI data to study the flow of CSF in Aqueduct of Sylvius (AS). The spatial domain was digitized using Immersed Boundary method (IBM) [39]. Pulsatile inlet velocity boundary condition is used, and their results show pressure drop of 1.02 Pa and velocity of 30.20 mm/s for cylindrical model; whereas for elastic wall model, the pressure drop of 2.91 Pa and velocity of 64.65 mm/s was recorded. In another case study [40] the authors proposed a 2D rigid model of HVS where the pressure drop of less than 2 Pa and velocity of 7.3 mm/s is reported. In yet another study [41] the authors constructed a simplified geometry of HVS to model the mechanical behavior of CSF. To drive the flow of CSF, oscillating wall of third ventricle was used whereas at outlet zero pressure boundary condition was applied. The study deduced that pressure increases in lateral ventricles due to aqueduct stenosis but no significant phase difference between wall motion and pressure was observed. Moreover, the CSF movement is influenced by the pathway of CSF through CNS and brain movement. In addition, the pulsatile nature of CSF is also due to the elastic nature of the Ventricular space, and due to the changes in systolic and diastolic pressure in each cardiac cycle [42]. One of the extensive and supportive studies on simple CSF flow in the HVS is documented in [43] where 3D Ventricles were segmented from MRI data with 1 mm voxel size using MIMICS. A commercial code of Fluent was used for CFD analysis. CSF is treated as incompressible Newtonian fluid. Pulsatile velocity inlet and zero-gauge pressure at outlet boundary conditions were used. The maximum velocity and Reynolds number was found to be 11.38 mm/s and 15 mm/s in cerebral aqueduct respectively. However, in this study the walls of ventricles are taken as rigid and effects of Fluid-structure interaction are neglected.

3.2.2. Structural Modeling of Brain Tissue

In view of the objectives of this thesis, the structural modeling of brain tissue vis-à-vis brain tumor response and ICP has not been explicitly modeled in view of what has been stated above. However, what we can look for in literature is the structural modeling of brain tissue in relation to other pathologies such as cerebral edema, hematoma etc. While one can only relate to these pathologies, but at the same time hereinafter we (keeping aforenoted in mind) would devise a methodology pertaining to this particular section of the thesis. Be that as it may, hereinbelow it would suffice if we paraphrase some studies in relation to other physiologies (excluding tumor).

Just to reinforce what cited above, that since brain tumor effects on the displacement of brain parenchyma have not been modelled explicitly, however, some other related pathophysiological parameters have been modelled. For example, cerebral edema poses the same challenge as the brain tumor and its relationship vis-à-vis ICP is modelled using FEM [44]. Edema is a condition in which fluid accumulates within a tissue abnormally. It can be caused due to any of the factors, and in the ibid study, authors designed a study to investigate the same and calculated the corresponding rise in ICP. A 3D finite element model of edema was designed using the solid phase equation as:

$$-G\nabla^2 u_i - \frac{G}{(1-2v)}\frac{\partial u_k}{\partial x_i x_k} = -\alpha\frac{\partial(\rho_f g z)}{\partial x_i} \tag{3.9}$$

Where G is the shear modulus given by G=E/2(1+v), v is the Poisson ratio, z is the elevation potential, and since no hydrostatic pressure is accounted for z=0 Since Edema involves a fluid accumulation, the authors have used the Darcy's law which describes fluid flow through the porous media. The equation provided by authors is given by:

$$S_\epsilon\frac{\partial p}{\partial t} + \vec{\nabla}.\left(-\frac{k}{\mu}\vec{\nabla}(p + \rho_f g z)\right) = -\alpha\frac{\partial}{\partial t}\epsilon_{kk} + Q_s \tag{3.10}$$

Where the term Qs represents the edema; and there is an additional term which is the negative strain rate on the right-hand side of above equation which compensates for the fluid phase of edema Qs. This study is quite relevant to the proposed research because the finite element method so employed can also be used to generate 3D models of brain including tumor. In another case study [45] correlation between intracranial pressure and external response due to head injuries was studied. In practice, ICP holds pivotal importance to analyze the responses of traumatic brain injuries to skull and brain tissues. A 2D finite element model was devised to study the vibrational

responses of the head and their response to the state of intracranial pressure. On one side of model, a harmless load was applied, and on the other side the response was measured with reference to ICP. Results depicted that intracranial pressure increased as external loading increases i.e. load to outer surface or skull. In yet another case study [46], the interactions of the CSF with reference to how it acts as a mitigating factor in reducing the impact of traumatic head injuries is presented. Nearest node finite element modeling was used to study the behavior of CSF in head injuries. The authors concluded that if the CSF is not present, then the buffer mechanism that cerebrospinal fluid provides will be absent and any injury can cause brain structures to deform. They concluded that the main role of CSF is to act as a buffer for brain tissues. Traumatic Brain Injury (TBI) is a serious accident which involves an injury to brain and the effect of it is a sudden rise in ICP which tries to offset the injury consequences. B. Yang et al [47] studied the impact of head injury and devised a FEM based model. The learned authors studied the effect of traumatic brain injury on the brain tissues and how ICP rises vis-à-vis impact of injury. The authors used a surface-based fluid model to study varying behavior of brain structures. The main assumption of the model is that it works better under condition that collision occurs in frontal region of the skull. CSF was modeled as hydrostatic fluid. The role of CSF was validated as a buffer—to provide a cushion for brain under injury. The validated results showed improved bio-fidelity. From simulation settings and modeling perspective, P. Young et al [77] provides a relevant brief for simulation framework using NRL-Simpleware and Abaqus for the readers in developing a finite element head model. Then there is a gamut of studies done on similar aspect on injury mechanics whose review here perhaps may not be relevant, but these are nonetheless helpful in devising framework insofar case relates to structural mechanics [78-84]. On the differences and effects of considering brain as homogenous or inhomogeneous structure and subsequent effects of stresses a relevant study is reported in [85]. Lastly, since brain injuries can induce shearing stress a rheological study of brain under shear stress is reported by [86]. These are but a few important works on the relatable title of this project. The main purport and import of these studies are that first we need to mathematically model the tumor growth through which different pressures are to be calculated. Second, these pressures are to be applied on the relevant tissue section and thereon combining fluid analysis into perspective, finding the interaction of CSF with brain ventricles and parenchyma. Structural modeling vis-à-vis just a force/pressure load may not be the accurate representation if one does not consider the fluid interaction. As stated previously, ICP is the differential of many parameters and among them

fluid pressures hold the key. Brain tissue is also incompressible according to Monro-Kellie doctrine therefore compression/compliance of brain will inevitably be limited hence any compliance needed will be coming from the fluid part and not the structure part. Needless to say, once the compliance mechanisms are exhausted then the structural part comes into the picture and the brain parenchyma may thereafter undergo a permanent deformation creating increased stresses inside cranium.

3.3. Fluid-Structure Interaction Modeling

In past, CSF modeling has been limited to a simple flow analysis by taking ventricular walls as rigid, ignoring completely the influence of deformable nature of ventricles, thus hindering in reaching towards a complete understanding of flow dynamics and tissue interaction mechanics. Another reason why this approach of modeling is problematic is due to the fact that by considering the walls as rigid, effect of the external forces such as that of brain tumor cannot be included into broader framework of how tumor effects the CSF flow parameters within the brain ventricles. Thus, a course correction in approach for modeling such situations is needed. FSI is one area which has been widely used in areas concerning inter se interactions in various Multiphysics problems, such as modeling the effect of tumor on the CSF flow profile and the resistance of the flow on the ventricle tissue mechanics. With regards to taking ventricular walls as deformable, much of the work is restricted to 2D modeling; and one of the study related to present discussion [48] proposes a 2D computational model of CSF flow from human ventricular system using FSI. 2D geometry was constructed using MRI images from 1.5 Tesla machine. FSI simulation was performed in ADINA software. CSF is treated as incompressible fluid. Pulsatile velocity inlet, based on cardiac heart cycle, and zero pressure at outlet boundary conditions are used. The authors have performed simulations on two models: 1) taking ventricle wall as flexible; and 2) taking wall as Rigid. The flexible wall model produced better results compared to rigid wall model as it could mimic the diastolic backflow. The maximum velocity in cerebral aqueduct for rigid and flexible model is found to be 11 mm/s and 8 mm/s respectively. The total pressure drop for rigid and flexible model is reported to be 3.5 Pa and -0.2 to 2.4 Pa respectively. Maximum displacement reported by the authors for the walls of ventricles is 0.006 mm. However, this study is limited owing to the approximation of assuming it as a 2D case. By modeling ventricular body in 2D, most non-linear interactions are missed out which are otherwise present in a full spectrum 3D modeling. Milan

Toma and Paul D.H. Nguyen [50] studied and devised a similar fluid-structure interaction model wherein analysis of CSF was carried out considering head model, so devised, subject to rapid changes in acceleration. They concluded *inter alia* that, subject to changes in accelerations, the volume of brain may undergo changes (or decreases) and volume of skull remains same; this change in volume causes CSF to fill in the spaces/void created due to deformation of brain. This study is relevant inasmuch as it relates to the compliance of CSF when brain structure undergoes deformation and also demonstrates, rather reinforces previous claim that CSF provides a cushioning effect to brain since fluid moves relatively faster than solid object. S. Cheng et al [51] provides yet another study which observes the fundamental effects of carrying fluid-structure interaction modeling on the flow of CSF in spinal subarachnoid space. This study may not be relevant but nonetheless provides a conclusion which is can be used here. It states that in spinal space the effect of either normal or stenosed CSF case (in cerebral aqueduct stenosis) have little effect on the flow or pressure of CSF in spinal cord subarachnoid space. This conclusion becomes relevant since I have, for the purposes of this thesis, ignored the cause/effect of including spinal cord (or spinal subarachnoid space) in two-way FSI model coming in subsequent section and this one of the ground as reinforced by [51] to not consider in cases for ICP evaluation.

In view of what has been discussed above, an irresistible conclusion sets forth which demands that a unified study is needed to be undertaken which takes into consideration the entire 3D ventricular body as deformable and records the effects of solid flexible walls on CSF fluid profile and vice versa. Finally, it is worthy to reiterate that the proposed study is a step towards modeling CSF flow in ventricles using FSI. In particular, it aims to address the question of how brain tumor can affect the CSF flow in the ventricles.

3.4. How to approach towards problem?

I have approached this problem by solving interdependent problems. First two scenarios are modeled wherein ICP can come into picture. First scenario entails modeling stenosis of cerebral aqueduct, as I have mentioned earlier one of high ICP causes is a stenosed aqueduct. Second scenario entails modeling brain parenchyma interaction of tumor while also considering CSF fluid forces. This makes the model complete. The above two scenarios provide us the necessary tools wherein we can study the ICP mechanics in both instances individually and as a whole as well.

3.4.1. FSI Modeling of Stenosis of Cerebral Aqueduct—A Conspicuous case of elevated ICP

This phase is an extension of earlier phase but model's a specific case which, needless to say, influences the outcome of elevated ICP in most cases. Stenosis of cerebral aqueduct poses a unique challenge in modeling thus this aspect has been carefully looked into, while taking the basic framework as it is. Again, a two-way fluid-structure interaction model is devised keeping in view of CSF-ventricular body interactions. At the same, the stenosis of aqueduct is ensured taking forces of tumor and applying on the aqueduct thereby exposing it to blockage.

3.4.2. Complete FSI Model of ICP

This phase begins with by modeling brain tissue modeling and incorporating it in the model of FSI developed above. This extension in scope is important because ICP is broadly inter-alia the resistance of brain parenchyma against ballooning pressure; the resistance and the pushback (towards the skull, needless to say) it gives to the increasing ICP. Thus, now at this juncture we would again be using the same FSI framework include tissue level modeling and here at this phase just include limited brain layers for the development of a fundamental framework and provide a complete description.

CHAPTER 4—MATERIALS AND METHODS

This chapter delineates the necessary steps in terms of materials and methods taken to achieve the objectives described above and fulfil the deliverables of the project. It also discusses some basic mathematical framework behind the methodology proposed herein.

4.1. Dataset Modalities and Preparation

This is a patient specific study so that a computational technique can be development. In this study, MRI image of 44 years old female patient diagnosed with brain tumor is used. The MRI image has resolution of 512 mm x 512 mm x 288 mm. The datum is obtained from INMOL Cancer Hospital[5]. All images (and different MRI modalities) are in Dicom format. Furthermore, it was by design and careful consideration that we **ONLY** considered a case wherein tumor was in early stages. We have not considered those cases where metastasis of tumor has reached to a stage where modeling of the same may not be fruitful. Software used for MRI data visualization is on opensource with the name MANGO[6] (Multi-image Analysis GUI) medical viewer.

4.2. Segmentation and 3D Reconstruction

For segmentation and 3D Reconstruction purposes, I have used 3D Slicer. 3D Slicer is an opensource software which gives various functionalities for automatic and semi-automatic segmentation techniques. Since I have relatively easier workload on the segmentation half therefore that is easily doable on 3D Slicer with good accuracy. On the reconstructed parts, Laplacian smoothing filter is also applied to remove unwanted and spurious segments or edges. Furthermore, all files for reconstructed are saved in STL file format for further processing.

[5] INMOL Cancer Hospital, Khayaban-e-Jamia Punjab Block D, New Muslim Town, Lahore, Pakistan.
[6] Software publicly available online and can be downloaded from <http://ric.uthscsa.edu/mango/> accessed 21st August 2019

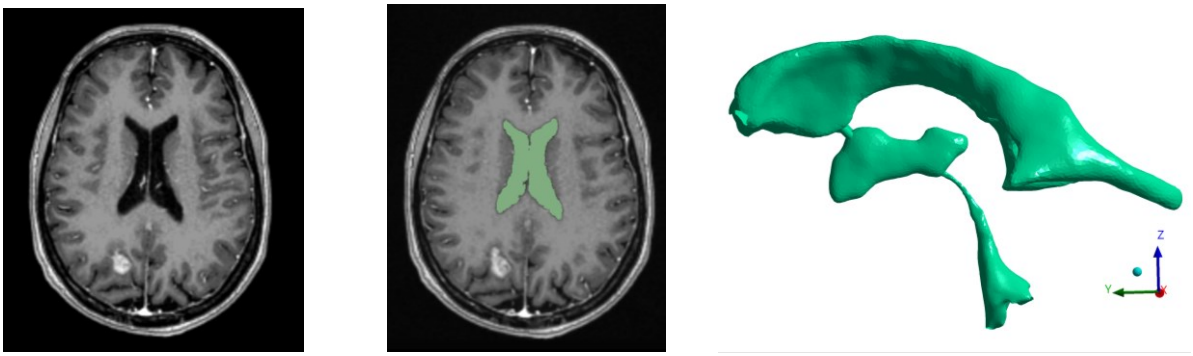

(a) (b) (c)

Figure 14. (a) original T1-contrast enhanced axial scan; (b) Ventricles segmented from T1-contrast enhanced axial scan; (c) 3-D reconstructed ventricles.

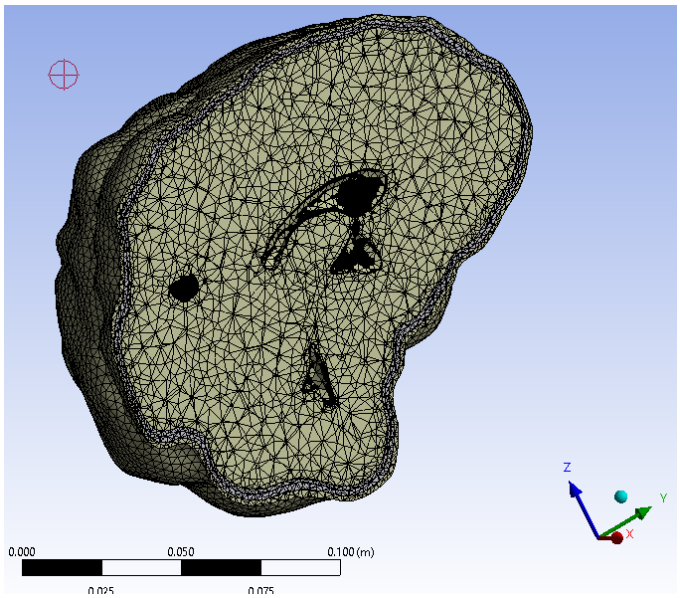

Figure 15 3D Reconstructed brain parenchyma and different brain layers.

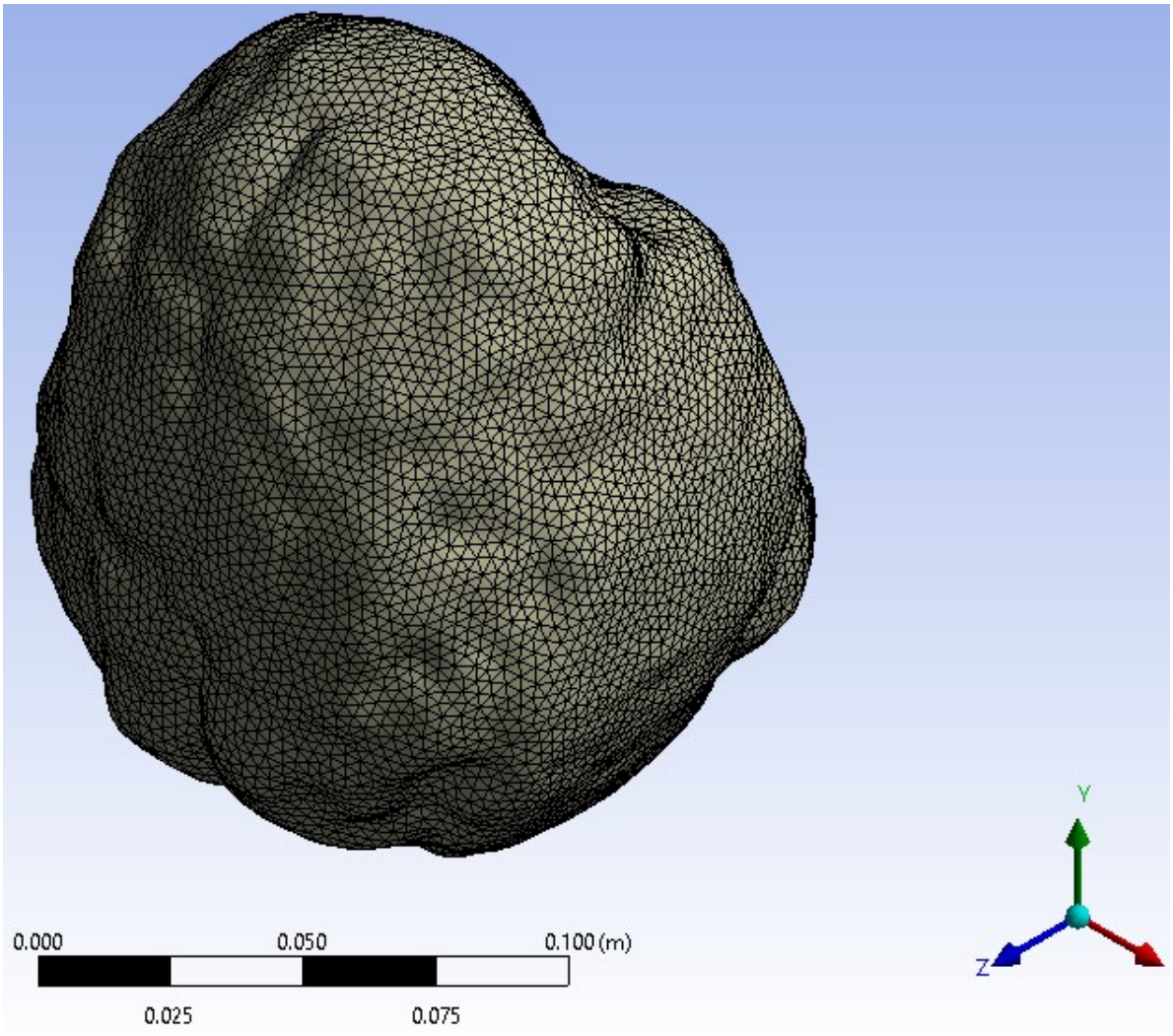

Figure 16 Full Brain 3D Volume

4.3. Tissue Level Material Modeling

Choosing correct material model to represent soft brain tissue is critical in the analysis. Most material models for brain parenchyma and ventricles have differed in literature. It is obviously clear that brain has a non-linear behavior for different loading conditions [99]. For example, some papers in literature have considered brain parenchyma as linear viscoelastic [99-101]. While others have considered brain as hyperelastic [102-105]. And in some papers the brain parenchyma is considered to have both hyperelastic and viscoelastic behaviors [106-108]. Furthermore, recent evidence suggests that soft tissues, such as brain, gliomas etc. have unusual

mechanical properties, especially under shear load [109-111]. The conditions stated in paper by [104] therein suggest hyperelastic models of Ogden and Mooney-Rivlin to perfectly full fill the brain shear loading criteria. Whereas, in some papers modeling traumatic brain injury (TBI) both viscoelastic and hyperelastic behaviors are used [112] which completely full fill both the criteria of large deformation of brain parenchyma and also of a damping behavior wherein shear relaxation (or creep) main occur in soft biological tissue such as brain parenchyma, tumor etc. Brain, in view of the foregoing, is modeled as hyper-viscoelastic. To model it as hyperelastic, one needs to find the strain density function which is basically the stored strain energy per unit volume.

Using finite strain theory, strain energy density function can be calculated. Without going into much detail, in generalized terms, to find the strain energy density function, denoted by φ, deformation gradient $\boldsymbol{F}$ needs to be calculated. Consider a body in undeformed frame X and undergoes deformation. The deformed frame is denoted by x (refer figure above). Then the deformation gradient F using finite strain theory can be calculated as follows [113-114]:

$$F = \frac{\partial x(X,t)}{\partial t} \tag{4.1}$$

The strain density function in terms of deformation gradient can be calculated as follows:

$$J = \det[F] \tag{4.2}$$

$$\sigma = J^{-1}\frac{\partial \varphi(F)}{\partial F}F^T \tag{4.3}$$

where σ is the Cauchy stress tensor, J is the Jacobian of the body and is defined in equation (4.2). Using this equation (4.3), the strain energy density can be calculated. Now the function φ is material behavior dependent. In this paper, we shall use Ogden 2-parameter hyperelastic model because as stated in [104] and [112] the Ogden material model fully explains the behavior of brain under various loading conditions. Ogden Model [115] formulated in terms of principal invariants (orthogonal vectors, Q) λ_1, λ_2, λ_3 and strain energy density function widely used in modeling biological tissues is given by:

$$\varphi = \varphi(\lambda_1, \lambda_2, \lambda_3) = \sum_{n=1}^{N}\frac{\mu_n}{\alpha_n}(\lambda_1^{\alpha_n}, \lambda_2^{\alpha_n}, \lambda_3^{\alpha_n} - 3) \tag{4.4}$$

Where N is the number of terms used in determining strain energy density function (such as Ogden 2 parameter or 3 parameter model), μ_n are material constants (shear moduli) and α_n are the experimental value (dimensionless), n= 1,2,3,….. N. Whereas, also In view of studies [53-56]

Table 1. Tissue Structural Properties

Tissue Layer	Density (kg/m^3)	Poisson's Ratio	Elasticity Modulus	Ogden Hyperelastic Model Parameters	Viscoelastic Model (Prony Series Constants)
Skull	1210	0.22	8.0 GPa	-	-
Ventricles	1000	0.49	30 KPa	-	
Dura Mater	1133	0.45	31.5 MPa	-	-
Brain Parenchyma	1040	0.4996	-	μ_1= 53.8 Pa, α_1=10.9, μ_2= -120.4, α_2=-12.9,	G_0= 12.5 KPa G_∞=1 KPa $\beta = 100\ s^{-1}$
CSF*	1000	0.49	Bulk Modulus= 2.19 GPa	-	-
Tumor	1040	0.4996	-	Same as brain parenchyma	Same as brain parenchyma

*as a structural layer representing subarachnoid space

and conclusion drawn therein the brain behaves as far as possible a viscoelastic material and therefore an elastic approximation would be inaccurate. A viscoelastic shear modulus is approximated using Prony series, as provided by [57] with shear relaxation with decay constant ζ and two constants G_0 and G_∞ where the former is instantaneous shear modulus and latter is the long-term or steady state shear modulus. A general Prony series for shear modulus thus can be presented as the viscoelastic property of the brain parenchyma is calculated using the Generalized standard linear model and approximated using Prony series shear relaxation which is given by:

$$G(t) = G_\infty + (G_0 - G_\infty)e^{-\frac{t}{\zeta}} \quad \textbf{(4.5)}$$

Where G_∞ is the long-term relaxed shear modulus, G_0 is the instantaneous shear modulus which would be high. The numerical values are listed in table 2. Brain tumor is also modeled with the same properties as that of brain parenchyma but with an additional shear stress due to increased stiffness of tumor core [116]. Ventricular body is modeled elastic and is consistent with the literature available on modeling it.

4.4. Fluid-Solid interface delimitation

To reconstruct data into 3D CAD models, brain ventricles and tumor core are segmented from MRI images manually, using 3D Slicer and MIMICS Inc; Laplacian smoothing filter is applied as a post-processing tool to smooth 3D CAD models. To setup the simulation, solid and fluid domains are set-up separately, where CSF is referred as fluid domain and ventricular walls as the solid domain. Fluid-solid interface boundary is delimited by creating a surface **Ωs** such that the surface acts as a coupling where two variables are transferred at each timestep: fluid domain transfers forces and structural domain transfers displacements to ventricular walls. FSI surface delimitation is primarily limited to the ventricular surface.

4.5. Numerical Simulation Method

Numerical simulation consists of application of various mathematical equations and predicting a response thereof. With the advent of computational modeling, solving complex models containing non-linearities have become relatively easier. In scenarios consisting of fluid-solid mechanisms such as the one at hand, the underlying case is a multi-physics problem embedding both CFD and Structural simulations. In subsequent paragraphs of the section, the simulation setup of the entire problem is described. First, I would dilate upon settings on the structural side, pertaining to settings such as meshing method and inter se connections of brain tissues. Evidently, since this project has been divided into four phases and in essence all have the same numerical method ergo I would not describe them individually rather collectively (and wherever a distinction has to be made I will mention therein); and brief tinge of mathematics is also included to make sense of the numerical method for the reader. Lastly, I have extensively used **ANSYS (both mechanical and fluent)**[7] in carrying simulations because I feel that it is relatively easy in doing complex multi-physics problems such as FSI.

4.5.1. Meshing

In the structural part pertaining brain and its constituent components, meshing is the most important part due to complex curvature structures which are evident in the figures of 3D reconstructed parts reproduced above. I may, at my convince, will briefly touch upon different

[7] ANSYS is a commercial and student software providing services for finite element modeling.

meshing schemes[8] available herein. The reader can easily understand why a particular scheme is used and not others. I will also clarify some aspects of 3D reconstruction of brain parenchyma and integration of different parts among them.

Starting with regard to 3D reconstruction I want to make here two points. First, the models so created require post-processing steps therefore I have used Laplacian smoothing filter provided by 3D Slicer. This is makes sure that mesh does not contain spurious or unwarranted noise. Second, the reconstructed are exported into STL file format which are further used in importing 3D parts in ANSYS. Every tissue, such as WM or GM, has a corresponding STL file which is imported in ANSYS Spaceclaim[9]. In geometry section, we have different parts which are either glued together in the beginning due to their proximity, adjacency or relevancy inter se to make sure mesh remain conformal[10]. *Shared topology*[11] is used to obtain conformal mesh across different section of 3D parts (especially at intersections). This conformal mesh at times is necessary so as to ensure consistency and reduce/eliminate unnecessary load on computational power, in other words improving optimization of mesh. Shared topology however can only be used where two 3D parts are either directly in contact; and wherever, the part is enclosed in other part then *merge topology*[12] can be used instead. Having set out the 3D reconstruction part, I now proceed towards meshing schemes. In ANSYS, broadly we have five types of meshing *viz*. (i) hexahedral meshing, (ii) patch independent meshing (unstructured mesh), (iii) patch conforming mesh (conformal mesh), (iv) all triangles meshing and (v) cartesian meshing. These methods are used in variety of ways and the combination of above may yield the desired conformal (or if non-conformal a smooth consistent mesh). Since I wanted to have relatively finer and consistent mesh therefore, patch conformal mesh is performed. At the contact faces, a moderately finer mesh is also done so that stress singularity can be avoided.

[8] More information about meshing methods can be searched at < https://ansyshelp.ansys.com/>.
[9] ANSYS Spaceclaim is 3D CAD Solid Modeling Software. More information can be searched at <http://www.spaceclaim.com/en/default.aspx>.
[10] A meshing scheme where consistency between elements and nodes is preserved by making the intersection of two elements a sub-set of it; and there should not be an intersection area or so as to say that the distance between shared edges must one (or equal to that edge).
[11] Shared topology is a mechanism which provides conformal mesh among joining bodies. More information can be searched at < http://help.spaceclaim.com/dsm/4.0/en/Content/ANSYS_SharedTopology.htm>.
[12] For more information see <http://help.spaceclaim.com/dsm/4.0/en/Content/ANSYS_SharedTopology.htm>.

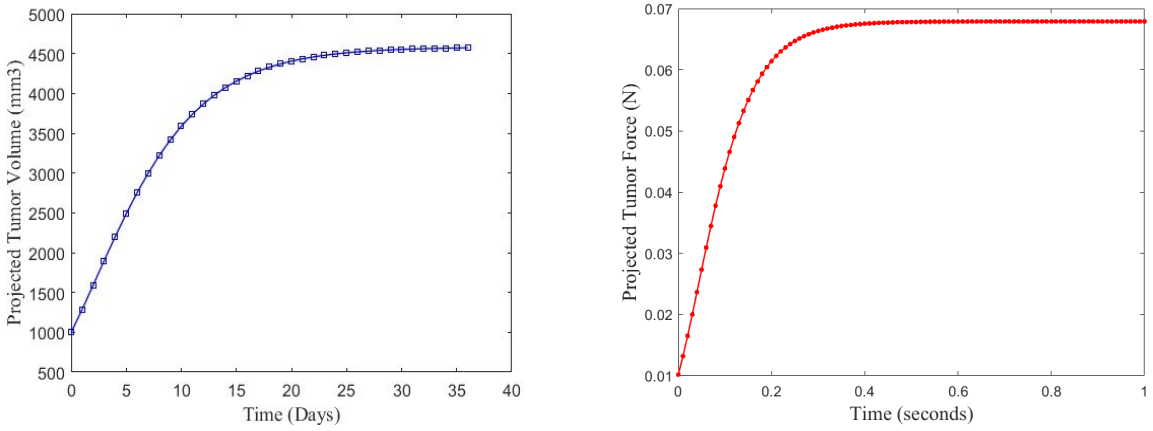

(a) (b)

Figure 17. Two graphs showing tumor growth and forces. (a) represents tumor growth using Gompertz model; (b) shows forces calculated using standard body weight formula.

4.5.2. Tumor Growth Modeling

As mentioned previously, tumor core is segmented from the MRI images manually. Needless to say, the initial tumor size needs to be grown in temporal spectrum so that the loading conditions can become dynamic in nature: this will depict the real-life scenario wherein forces no longer remain static. To predict the growth of tumor, Gompertz mathematical model is used which is one of the widely used models to extrapolate tumor cells based on the initial tumor volume [70]. The model has the solution in the form as:

$$\boldsymbol{V(t) = V(0)e^{\frac{\alpha}{\beta}(1-e^{-\beta t})}} \quad \textbf{(4.6)}$$

where, V(0) is the initial tumor volume, α and β are the initial proliferation rate and the exponential decay constants which have values of 0.279 and 0.1470 (values taken from study of [71] in which authors did a study on the dataset of [72]) respectively, and t is the time in days. While the efficacy of these models on humans is still an ongoing effort and needs to be gauged objectively because of the inadequacy of in-vivo measurements of tumor size over time, various models such as those aforementioned, however have mostly relied on animal studies such as those done on mice et cetera to find the constant values. While experimentally these growth constants may not actually depict about the exact nature of tumor growth in humans, nonetheless they do provide valuable insight and a starting point in studying tumor growth pattern. With regards to tumor forces, it is generally

understood that tumor content is not fully a solid core [73], it also contains hydrostatic forces of fluid. However, for simplicity we have ignored the action of fluid forces and have only considered the solid core (which is also the extracellular matrix of the tumor). Body forces is one parameter which can address the concern of finding the forces of solid tumor core. Body forces can be thought of as forces acting on entire volume of body such as those of electric fields or forces due to the gravity. Forces due to gravity are basically the weight of the body and can be given by equation (4.7) as:

$$\boldsymbol{F = \int_V \rho g dv} \quad \textbf{(4.7)}$$

where F is the body force, ρ is the density of the tumor mass which is taken to be 1040 kg/m3 [74], g is acceleration due to gravity (9.81 m/s2) and dV is the volume differential element (graph of force in figure below).

4.5.3. Boundary Conditions

This section will describe boundary conditions of the problem. There are again two sets of boundary conditions, one pertaining two FSI problem for ventricles and other relating to the brain-ventricle interaction. I would herein describe both of these in different sections to remain consistent.

A) Boundary conditions relating to FSI on Ventricle-CSF

As shown in fig. the model consists of two inlets and two outlets. Inlets are defined in lateral ventricles with holes of 3.54 and 3.24 diameter. Outlets are defined in foramina of Magendie and Luschka. Mass flow inlet boundary condition with bulk production of 500 ml/day or 6.25x10-6 kg/s [48] is used to mimic the real-life scenario of CSF production. While at the outlet, zero-gauge pressure boundary condition is used to make sure that the outlet remains at a fixed static pressure. Physiologically, CSF production (or volumetric flowrate) has a constant bulk production given above, but also has a pulsatile component due to cardiac-induced systole-diastole movement. The pulsatile component is ideally a linear combination of sinusoidal harmonics given as [75]:

$$Volume\ Flow\ rate = Bulk\ flow + Asin(wt + a) + Bsin(wt + b) \quad \textbf{(4.8)}$$

In above, bulk production equals to 0.3 ml/day ($6.25x10^{-6}$ kg/sec), A is equal to 0.21 ml/min ($3.5x10^{-6}$), and B is the part of second harmonic and is taken with an amplitude of 0.05ml/min

Table 2. Boundary Conditions fluid domain

Boundary Conditions	Value	Reference
CSF Density	1000 kg/m^3	Masoumi et al [48]
CSF viscosity	0.001003 Ns/m^2	Redzic et al [69]
Bulk mass flow	6.25x10^{-6} kg/s	Wright et al [8]
Pressure outlet	Zero Pascal	L. Howden et al [43]
Modulus of Elasticity	30 KPa	Masoumi et al [48]
Ventricles Tissue Density	1000 kg/m^3	Masoumi et al [48]
Poisson's ratio	0.49	Masoumi et al [48]

(values taken from [75]. Carotid artery taking blood towards heart has zero phase difference ibid, similar to the CSF flowrate phase in C-2 vertebral column level [75]. However, CSF velocity in the cerebral aqueduct has a phase difference.

B) Boundary conditions relating to FSI on Brain-Ventricle interaction

The boundary conditions relating to brain-ventricle interaction have inter-alia two components. First, the connections of various brain (segmental such as gray matter, white matter etc.) tissues connections need to be defined. Some tissues need to be constrained and others given a separation layer etc. I intend to first throw a light on these herein in detail because if the connections and constrained inter se brain layers is faulty or undefined, the simulation results would not be what we expect.

In ANSYS[13], we have broadly four connection settings (or should I say how two objects are connected among themselves). Among them, I will be using three contact layer settings which are needed to completely define the problem. I have already discussed supra which layers of brain I will be using, so will not repeat them here.

(1) Between Skull and Dura matter bonded layer contact is used because it glues (or constraints) the two objects. This is need otherwise penetration of layers may happen.

(2) In the same vein, Skull is constraint and is fixed with all rotational and translational degree of freedoms $U_X=U_Y=U_Z=0$.

[13] For Meshing and Connection settings, see ANSYS documentation.

(3) Between CSF and Dura matter I have used no separation layer because this layer allows linear (relative) translation of both layers among themselves and at the same time no penetration is allowed.
(4) Tumor layer is defined as (deemed to be) in bonded contact with brain parenchyma.
(5) CSF layer is applied four different pressures of ICP (more to this later).
(6) Initially, during the course of study and for the purposes of designing a framework (or pipeline) I used only simplistic model containing few brain layers so that a behavior relatable can be identified. Therefore, for initial model I only glued (or bonded layer) the gray matter and white matter among them which results are report in coming chapter.
(7) Subject to point 5, CSF and brain layer have a contact layer of a frictional contact with coefficient of 0.2 (reference). Ventricular body has a bonded contact with the brain parenchyma. Since ventricular body (or to be precise its surface) is the fluid-solid interface therefore, it has to be bonded contact.
(8) Keeping point 6 in view, and subject to results obtained thereof, I proceeded therefrom towards a more realistic model which anatomically realistic insofar that it now contains different layers such as gray matter and whiter matter etc. Since inter se tissue connections such as gray and white matter are for the purposes of this study glued and have a bonded contact therefore, if explicitly stated otherwise, all brain parenchyma tissue such as gray matter, white matter, brain stem, cerebellum and others are defined with a bonded contact. The list of connections in a tabular form is provided herein below.

I now proceed towards boundary conditions used in this specific simulation. As stated earlier, skull is fixed in space and also the inlets and outlets of ventricles are fixed for translation and rotation. A constant pressure of various values is applied at the CSF layer to depict the nominal ICP inside the cranium. Tumor pressure (in terms of body weight only) is also applied at its position. FSI interface is defined, as discussed above, on the ventricular surface. Both fluid and solid simulations are coupled using ANSYS system coupling toolbox and data of forces and displacement is transferred at each timestep.

4.5.4. Fluid Part Solution Method

To solve the flow equations Fluent is used which uses Finite Volume Method (FVM) (by assuming a control volume in which flux remains conserved—taking divergence of flux equals to

zero) which, in principle, converts or reduces all the partial differential equations into a set of linear simplified algebraic equations. The underlying principles of any CFD solver primarily base on the Navier-Stokes' equation. The NS equation fundamentally rest on solving the continuity (4.9) and conservation of momentum equation (4.6) given as below [76]:

$$\nabla.(\rho.\vec{v}) = 0 \tag{4.9}$$

where ρ is the density of fluid (read CSF), v is the velocity of the fluid, ∇ is the gradient operator. And momentum equation is given as:

$$\rho\frac{\partial\vec{v}}{\partial t} + \rho(\vec{v}.\nabla)\vec{v} = -\nabla P + \tau\rho + \mu\nabla^2\vec{v} \tag{4.10}$$

where ρ $(\partial v \vec{})/\partial t$ is the local acceleration of fluid particles, ρ(v $\vec{}$.∇) v $\vec{}$ is the convective acceleration, ∇P is the pressure gradient, τρ are body forces, μ∇^2 v $\vec{}$ is the viscous term which resists the motion of the fluid particles. In (4.5) local acceleration is the change in velocity at a given point in a flow field; whereas convective acceleration is the change in velocity due to change of position of fluid particles in a fluid flow due to any unsteadiness along the streamlines.

Solving above equations requires spatial and temporal discretization together-with pressure-velocity coupling schemes which can be used to interpolate pressures at the faces of a control volume. Pressure-based solver is used with PISO (Pressure-Implicit with Splitting of Operators) coupling. For spatial discretization, second order pressure, and for momentum second order upwind is used. For gradient discretization, least square cell-based method is used. Implicit formulation is used in discretizing equations. Implicit time marching scheme is used using second order backward Euler derivative formulation. Implicit formulation is used in discretizing equations and equations are linearized and solved iteratively using present and previous values. This results into N equations for each cell. An implicit equation solver, based on Incomplete-Lower-Upper (ILU) factorization scheme, together-with Algebraic Multigrid method (AMG), is used to speed up the convergence of the solution. V-Cycle Multigrid method is used with a termination criterion of 0.1. For transient simulations, implicit time marching scheme is used using second order backward Euler derivative formulation, in conjunction with an additional stability criterion based on Courant-Friedrichs-Lewy number (CFL). It is calculated by (4.11) as:

$$CFL = \vartheta\frac{\Delta t}{\Delta x} \tag{4.11}$$

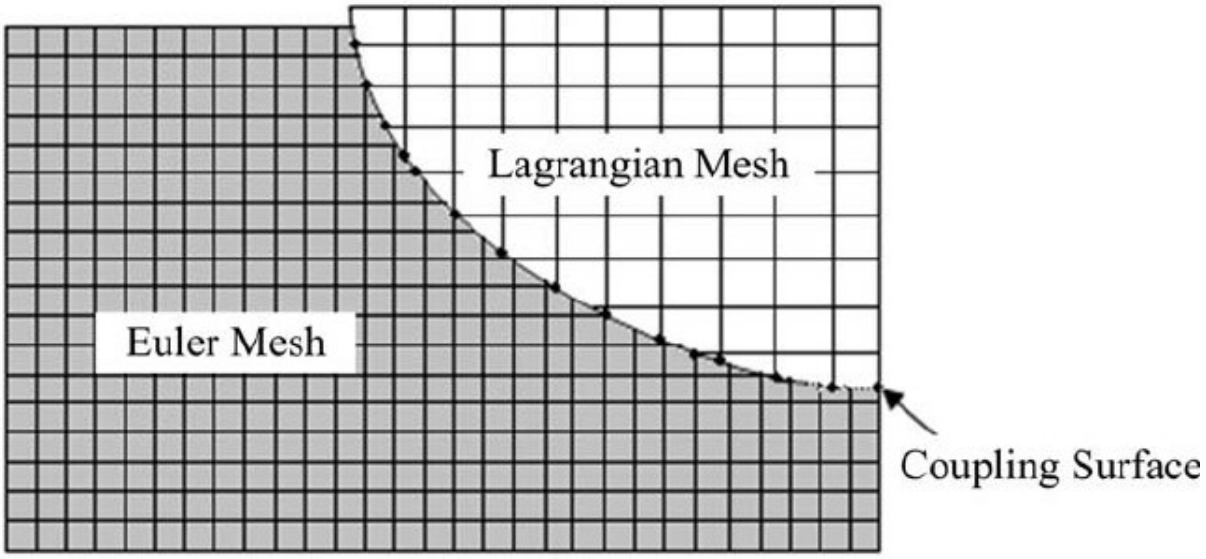

Figure 18. FSI coupling mechanism

where ϑ is the velocity, Δt is timestep size and Δx is the smallest cell size of control volume. There are furthermore additional parameters which merits determination and I for brevity will discuss them hereunder insofar they particular relate to fluid part.

Dynamic Meshing

Due to deformable boundary the elements can get distorted and thus losing their ideal shape, therefore dynamic meshing is needed so that the moving cells can be re-meshed correctly thereby preserving shape quality. Remeshing is used to keep the mesh parameters such as skewness, aspect ratio and orthogonal quality in acceptable quality range. Diffusion-based smoothing is used to smooth deforming cells. Following equation is used for smoothing.

$$\nabla.(\gamma\nabla\vec{u}) = 0 \quad (4.12)$$

$$\gamma = {}^{1}/_{d^{a}} \quad (4.13)$$

where γ is given as 1⁄d^a with d being the normalized boundary distance and a is the diffusion parameter and u ⃗ is the mesh displacement velocity.

FSI Coupling Mechanism

Once the individual solvers and domains are setup, system coupling is used to exchange data at each time-step to ensure strong coupling mechanism. Two popular methods for FSI coupling mechanisms are monolithic methods and partitioned methods [89]. Monolithic schemes provide standalone FSI simulation within single solver. Partitioned methods base their physics on solving solid and fluid domain independently of each other and coupling them via interpolating

scheme at fluid solid interface ΩS. The coupling interface must satisfy two important conditions i.e., the kinematic coupling condition and the dynamic coupling conditions [90]. The kinematic coupling condition concerns with the coupling of kinematic quantities such as velocity. The dynamic coupling conditions provide necessary conditions for forces to balance at the coupling interface. In case of ventricles, the thin shell structure serves as the fluid-structure interface. In the proposed scheme, the kinematic coupling condition is no slip condition. The mesh that is created at the coupling surface in strictly a one-dimensional problem looks something like **above (figure[14]).**

Timestep Size and Convergence Criterion:

To ensure true convergence, timestep needs to be same in both the solvers so that data exchange occurs at same instance. To this end, we have calculated timestep size based on the complexity of small-scale physics. A possible scenario for calculating a reasonable time-step size is by considering the cardiac-induced pulsations which would amount to taking smallest time-step size which is calculated using relation of $\Delta t=1/20f$, where Δt is the time-step size, and f is the frequency of heart beats. For a normal case, heartbeat ranges from 60-100 bpm. Equivalent frequency of 60 bpm equals 1 Hz and using (12) Δt equals to 0.05s. In this study we have taken a time-step of 0.01 seconds which is smaller than the above calculated threshold to capture small changes in the simulation. In FSI simulations executed using partitioned methods, convergence is an important variable which merits major focus. Local convergence in both structural and fluent solvers, and global convergence in the system coupling matter since it is probable that solvers may independently be converging but may not be converging inter se. System coupling toolbox of ANSYS provides coupling iterations within each timestep so that not only both solvers get converged but also a relative convergence tolerance is achieved, which in our case is set to 0.0005; while 5 coupling iterations are used per timestep with end time set to 4 seconds.

4.5.5. Structural Mechanics Setup

This section pertains to purely structural mechanics part (in other words ANSYS Mechanical) and I have again for the purposes of reader have differentiated this step into two distinct parts. One that relates to FSI surface for ventricle, and the other relates to the brain tissue

[14] Image taken with from [91]

simulation setup. I will also discuss some connected matters which are also needed to make sense of this section.

Structural Mechanics Setup—FSI surface of Ventricle

The structural domain is discretized into finite elements where equations are solved at nodes and interpolated at faces. The fundamental equation is given as below.

$$\sigma = E\varepsilon \tag{4.14}$$

where E is the elastic stiffness matrix, ε is the strain vector and σ is the stress vector. Newmark Integration scheme is used to solve equations because the model generated in our scheme has non-linearities in it, therefore implicit solver is needed to reach towards a solution in an iterative manner.

Structural Mechanics Setup—FSI for Brain tissue

As discussed above, the FSI interface for CSF-Ventricle is the wall/surface of ventricle which acts as a surface where data transfer occurs. The above equation (4.10) can only be used for linear materials however for hyperelastic materials such formulation won't work. Likewise, as noted above, solid domain is discretized using SOLID 187 and SHELL 181 elements and solved in ANSYS Transient Structural module. For large strain elements such as brain parenchyma, finite strain theory is applied to find element matrices and load vectors using updated Lagrangian method as follows:

$$[\bar{K}_\iota]\Delta u_i = F_A - F_R \tag{4.15}$$

where F_A is the applied force and F_R is the Newton-Raphson restoring force vector. $\bar{K}_\iota$ is given as follows:

$$[\bar{K}_\iota] = [K_i] + [S_i] \tag{4.16}$$

Where K_i is the stiffness matrix obtained through applying generalized stress strain law of elasticity as follows:

$$[K_i] = \int [B_i]^T [D_i][B_i]dV \tag{4.17}$$

where B_i is the strain-displacement matrix in undeformed frame of reference X and D_i is the stress-strain matrix. While S_i is the stress stiffness matrix given as follows:

$$[S_i] = \int [G_i]^T [\tau_i][G_i]dV \tag{4.18}$$

where G_i is the matrix shape functions, τ_i is the Kirchhoff stress tensor related to Cauchy stress tensor by Jacobian of the deformation gradient J as given in equation (3). Newton-Raphson restoring force is given by:

$$[F_i^{nr}] = \int [B_i]^T \sigma_i dV \quad \textbf{(4.19)}$$

Since we are extending the previous case wherein FSI surface was just wall of ventricles, now herein we are also including brain parenchyma interaction, therefore the surface of FSI will now consists of two cases. First is the surface of ventricle wall supra, and second is the connection of meshes between the adjacent brain parenchyma tissue and to the walls of ventricles. Since contact points will be generated, these would act as a source for transferring displacements and stresses through the brain parenchyma tissue. Solver types is adjusted according to the convenience and according to the degrees of freedoms of the mode. Ideally Direct Solver is computationally expensive but solves the model entirely at once, however PCG (Pre-conditioned Conjugate Gradient) solver is an iterative based solver and decomposes the domain into different scales and builds mathematical model iteratively. As I will describe below, the computational needs of this thesis in terms of all solvers, this point shall be addressed there.

To judge the convergence of solution Newton-Raphson method is used which is given as below:

$$x_{n+1} = x_n - \frac{f(x_n)}{f'(x_n)} \quad \textbf{(4.20)}$$

Above equation (4.20) is used to converge forces, moments and displacements at each time-step, which works by the principle that the energy added due to the external loads must eventually balance the energy induced by the reaction forces. Full Newton-Raphson is method is used and force, displacement and moment convergence is monitored for any unconverging solution. Timestep size as mentioned earlier is used 0.01 seconds.

CHAPTER 5—RESULTS OF ICP AND STENOSIS OF CEREBRAL AQUEDUCT

In this chapter, simulation results of each phase (herein phase 1 and 2 in chapter 6) targeting the objective of this thesis are presented. It is important to mention that since the Stenosis of cerebral aqueduct is closely related to devising a basic framework therefore, to eliminate repetition, the results of stenosis of cerebral aqueduct as they resemble (or in stricto sensu go hand in hand with phase 1). Stenosis of cerebral aqueduct is produced by applying a tumor force on the walls of aqueduct and the results thereof are produced hereinafter. (For the purpose of this chapter Cerebral aqueduct shall be referred to as "CA").

Case study 1—Simulation Results & Synopsis of Stenosis of Cerebral Aqueduct

5.1. Model Validation

Simulation setup defined in chapter 4 (supra) is executed for 1 second. Inlets are supplied with mass flowrate and velocities across various sections of ventricles are recorded for the case of aqueduct stenosis. Additionally, a normal case is also executed without any external force to visualize the relative effect of tumor and its contribution towards aqueduct stenosis. Model is validated by comparing the results of segmentation against those given by the radiologist. The model is validated with a reasonable accuracy and minimum error. Table shows the results of model validation.

Table 3. Model Validation Parameters

Specimen	Ventricular Volume			Tumor Volume		
	Segmented Volume (ml)	Ground truth Volume (ml)	Percentage error	Segmented Volume (mm^3)	Ground truth Volume (mm^3)	Percentage error (%)
MRI Image	25.32	24.32	4.18%	997.29	959.51	3.93%

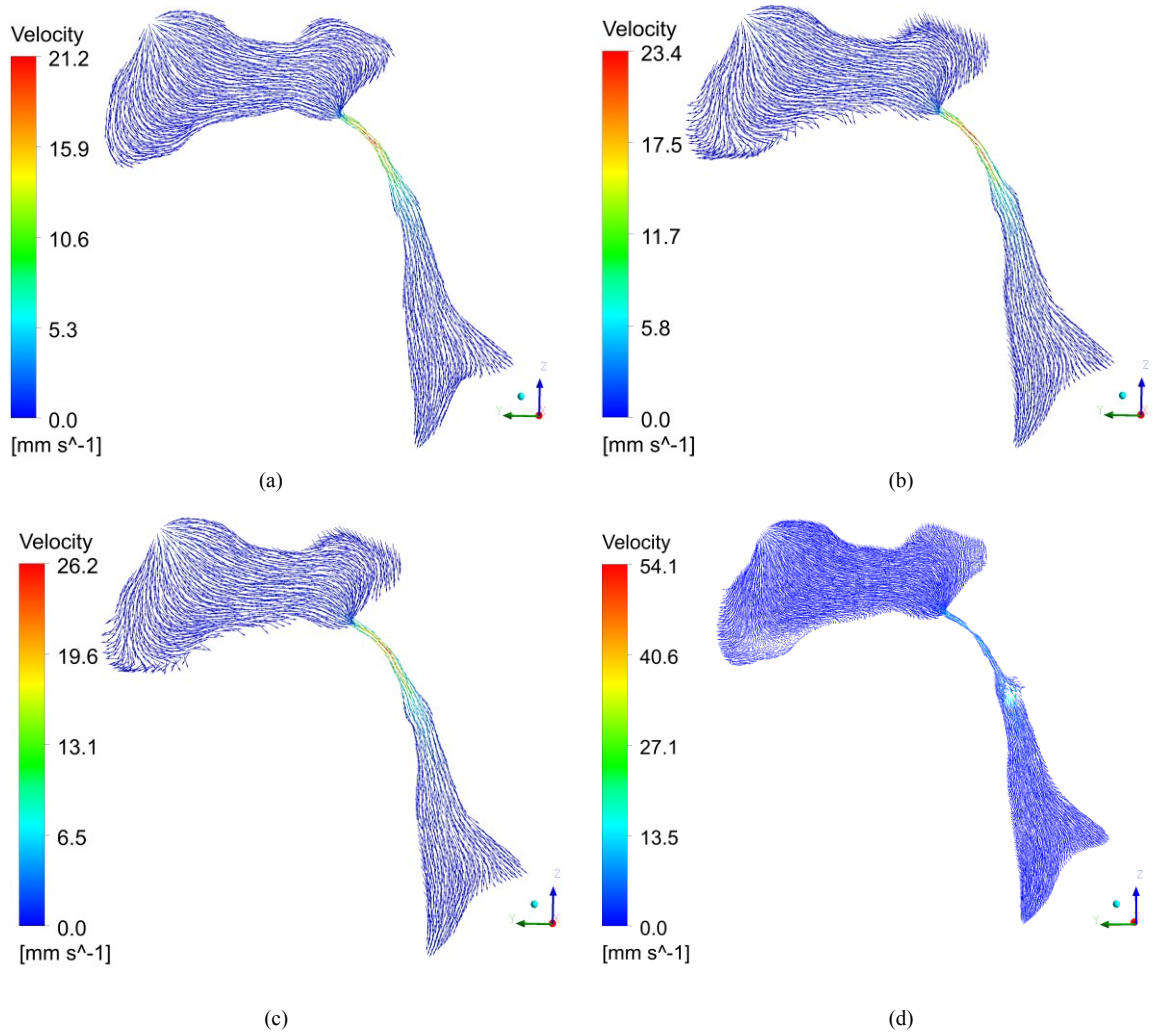

Figure 19. (a) Maximum velocity when no external force acts; (b) Velocity in CA at timestep 0.1s; (c) Velocity in cerebral aqueduct at timestep 0.5s; (d) Velocity in cerebral aqueduct at 0.75s shows considerable constriction in aqueduct where velocity vectors start to distort.

5.2. Flow Parameters—Velocity and Reynold's Number

Velocity field is an important parameter which greatly influences the outcome. Needless to say, peak CSF velocity occurs always occurs in the cross-section of CA due to decreased pathway and according to the continuity law. Herein we present the simulation results for two cases. First case pertains to FSI simulation of ventricular body with no interaction of tumor forces. Vector plot of CSF velocity in third ventricle and CA is presented in figure 19 (a). Peak CSF velocity across the CA for aforenoted case is found out to be 21.2 mm/sec. This is consistent with both the previous FSI-based papers and PC-MRI studies found in literature (discussed later). This result datapoint is reported to visualize the inter-se differences. Figure 19 (b), (c) and (d) show

vector plots of velocity in third and fourth ventricle for cases wherein tumor forces are applied on walls of CA to ensue different levels of stenosis. The stenosis occurs at different timesteps hence associated timestep is also reported. Figure 19 (b) pertains the case when there is 10% stenosis of CA hence a steady rise in CSF velocity is observed. This case repeats steadily for the case of 45% [figure 19 (c)] stenosis hence not much difference is observed in terms of velocity. However, after certain stenosis level, in this case 75%, [figure 19 (d)] the velocity rises sharply and reaches to 54.1 mm/s depicting that the duct has deformed considerably relative to the previous stenosis levels. In addition, if one observes closely figure 19 (d), one can easily notice that the velocity vectors at the point of force application have started to change direction as well which clearly suggest, as noted earlier, that this (and beyond) stenosis level ensue stenosis of CA considerably. This also reaffirms our earlier proposition above that the deformable property of ventricle ought not be overlooked because it has visible effect on the biomechanics of the system. In addition to the aforementioned, another useful parameter to gauge the dynamics of CSF under the scenario of stenosis of CA is to find out Reynold's number of the flow. Reynold's number is an important parameter which signifies the transition of flow from laminar to turbulent. It is given by:

$$Re = \frac{\rho \vartheta D}{\mu} \tag{5.1}$$

From equation (5.1), Reynold's number has a directly proportional relationship to the velocity which also suggest that as flow velocity increase, so does the Reynold's number. Flow in lateral ventricles is in order of 10^{-3} mm/s which clearly shows characteristics of creeping flow. Consequently, in terms of Reynold's number in lateral ventricles there is no noticeable effect. However, flow velocity in CA cross-section changes abruptly and so does the Reynold's number. While for case presented in figure 19 (a), Reynold's number is found out to be 38.5, however, for the case presented in figure 19 (d) where 75% stenosis is ensued it goes to 110. Laminar flow is characterized (for flow in pipes) according to Reynold's number where if Re<2500, the flow profile is said to be laminar. While the Reynold's number found out herein are less than the above-mentioned threshold, however, when observing it in high curvature cross-sections such as CA, even a low Reynold's number may not preclude a localized turbulence in the aforesaid region. In any case, a stenosed CA represent a complex situation wherein flow profile, velocity and Reynold's number change significantly and may pose clinical complications.

5.3. Structural Parameters—Pressures and Deformation field

Pressure is an important fluid dynamic variable which drives flow through any media via pressure differential. Ventricles are cavities containing CSF fluid, hence pressure of CSF on the walls of ventricles is an important parameter which needs consideration. If one observes closely [see figure 14 (a-c)], ventricles are four interconnected cavities connected through different channels such as foramen of Monro and CA. Among them, lateral ventricles are larger in volume and space, and the rest are relatively smaller than lateral ventricles. Hence pressure gradient and amplitude ought to be larger in lateral ventricles which is also observed in the case presented hereinafter. A larger pressure variations also determine the Transmantle pressure which is the net pressure gradient across the parenchyma all the way till the subarachnoid space. Resultantly, if Transmantle pressures are high due to high intraventricular pressure then one may also be confronted with the case of elevated ICP. Simulation results presented herein determine whether Transmantle pressures increase under the case of stenosis of CA, comparable to that of non-stenosed duct which would also depict a corresponding difference in cases for elevated ICP, if any.

Figure 20 (a) and (b) shows results of pressure field distribution on walls of ventricles. Figure 20 (a) pertains to the case of non-stenosed ventricles (no tumor force). In this case, a maximum pressure of 2.5 Pa is observed which is well validated with those in the literature (discussed later). It is also observable that the pressure variations in large cavities such as lateral ventricles are found to be spatially uniform due to their huge size. Pressure drop of 0.2 Pa and 1.7 Pa is found across the third ventricle and CA. A large pressure drop across the cross-section of CA is natural since fluid enters into a narrow pathway resultantly greater pressure drop is needed to drive the flow downwards and according to continuity law, velocity should also resultantly increase, as seen above. Figure 20 (b) pertains to the case wherein pressure field is reported for a stenosed CA. In this case, a higher pressure in lateral ventricles is observed due to the increased inflow (or due to decreased outflow) towards lateral ventricles. Maximum pressure of 5.4 Pa is found in the lateral ventricles, with a pressure drop of 0.8 Pa in the third ventricle. Pressures in cross-section of CA present a unique case. A stenosed duct is practically a duct which is squeezed to a point where ideally there is no outflow. Hence, beyond that point (post stenosed section) no fluid enters which makes pressure in that section to drop below the surrounding pressures. This confirms that under stenosed CA, pressure in the CA and fourth ventricle drop significantly and pressures in lateral ventricles increase, indicating distention of lateral ventricles. Values of

pressures obtained under stenosed CA case are reported and compared with other papers based on CFD and FSI analysis in discussion section.

Figure 20 (c) shows wall shears on the walls of CA and fourth ventricle. Wall shear stress is an additional parameter which is needed towards analysis. All fluids of engineering interest are viscous fluids and most follow Newton's law of viscosity. In other words, friction and viscosity are interchangeable. Low viscosity means that the fluid layers that are overlapping have low internal friction and can slide easily without the loss of energy. The parallel force of fluid on the walls of ventricles is called the shearing force and the stress generated thereof is called shear stress. Since in a stenosed CA, force is applied on walls of CA, this causes fluid layers to abruptly overlap each other, in the localized region, causing the derivative of normal component of velocity (du/dy) change significantly resulting in high shear stresses (using equation 1), since dynamic viscosity is same. A non-stenosed CA does not give high wall shear stresses (has stresses of order 10^{-2} Pa) which suggest that normally CSF flow has laminar profile. However, when the structural force is applied on the walls of CA, shear stress so generated amounts to 25 Pa which is quite significant. This additional parameter may also aid in broader understanding.

Since walls of ventricles have been modeled as elastic therefore their deformable character results in deformation on walls of ventricles. Figure 21 (a) and (b) show the deformation field obtained on the walls of ventricles under two cases. Figure 21 (a) pertains to the case of non-stenosed walls of CA. It shows a usual and nominal deformation of 2 um (0.002 mm) which is negligible for practical purpose. Masoumi et al [32] reports for their 2D modeling around 0.006 mm hence deformation obtained herein is well validated within the normal case. Figure 21 (b) shows the case wherein tumor force (at 75% stenosis level) is applied to ensue stenosis of CA. In this particular case, a drastic increment in deformation of 0.146 mm in lateral ventricles is observed. This deformation shows that once the CSF flow is obstructed considerably, pressure in lateral ventricles increase (as discussed above) and deform the lateral ventricles. Not only this, it also creates a requisite compliance for the excessive retention of CSF fluid which cannot flow towards fourth ventricles due to constriction. Since this particular case has not be modeled even in 2D hence the values presented herein can only be interpreted intuitively.

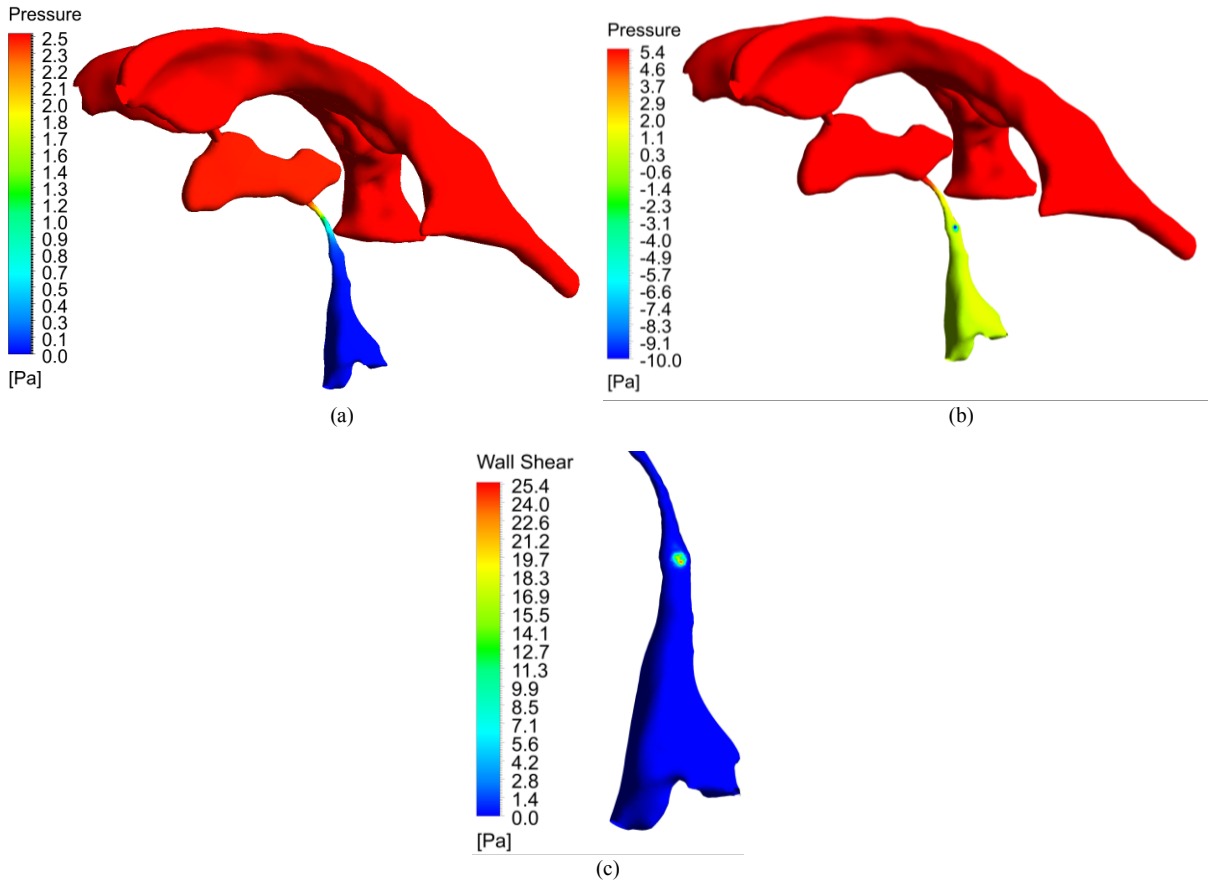

Figure 20. Pressures on the walls of ventricles. (a) shows pressure distribution on the walls of ventricles when no tumor force acts; (b) shows pressures on the walls of ventricles when tumor force acts; and (c) is the wall shear created due to tumor force.

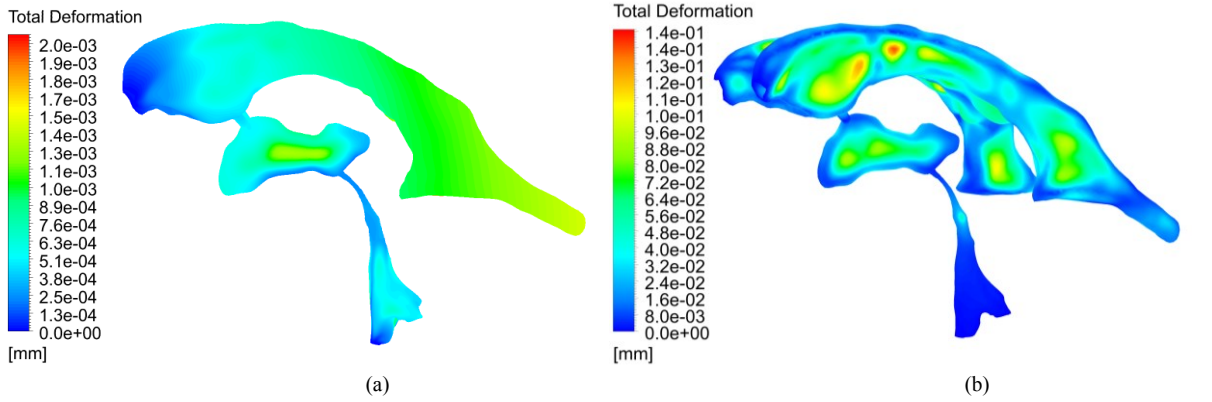

Figure 21. Deformation distribution on walls of ventricle. (a) shows deformation when no tumor is acting, (b) shows increased deformation due to the action of tumor force.

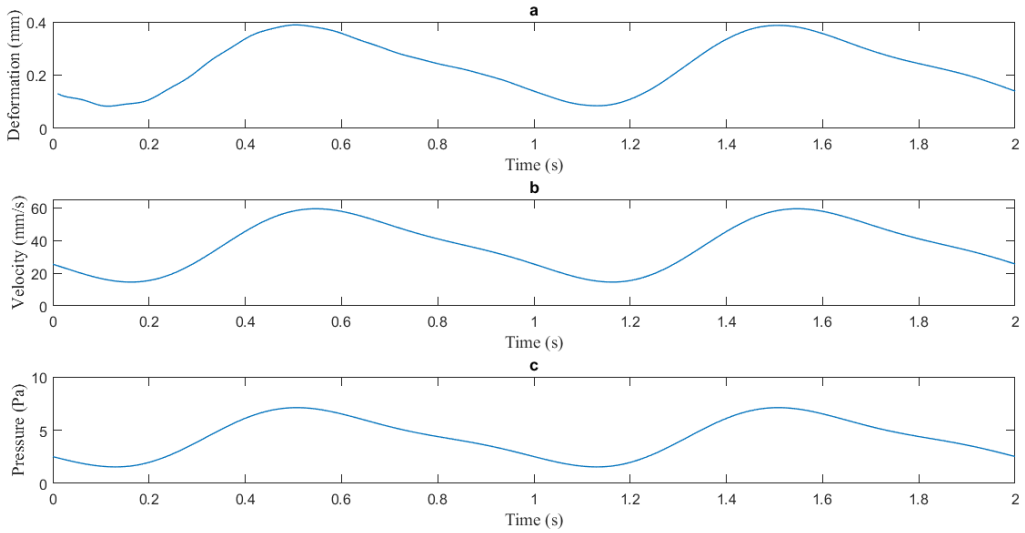

Figure 22. Graphs of Deformation on walls of ventricles (a); velocity in the Cerebral aqueduct (b); and Maximum pressure variation in lateral ventricles.

5.4. Effect of Pulsatility on Stenosis of Cerebral Aqueduct

The pulsatile component of CSF is induced due to the blood flow in cerebral vasculature during a cardiac cycle. The equation which governs this is given by equation (4.8). To give CSF a pulsatile component as given in aforesaid equation, a User Defined Function ("UDF") was written (in C-language). The case was simulated for two seconds (to visualize correctly the behavior in terms of graph). Pulsatile mass flow inlet is provided using equation (4.8). Results obtained using pulsatile component are provided in figure 22 in terms of velocity, pressure and deformation graphs. Figure 22 suggest that the pulsatile component of CSF has drastic influence on the CSF velocity which goes up to 58.21 mm/s. It is understandable since the motion of cerebral vasculature pushing and driving CSF flow creates additional force which produces motion of CSF in ventricles. Deformation observed on the walls of ventricles does increase when considering the pulsatile nature of CSF. As stated above, the deformation observed on the walls of ventricles under the stenosed CA is 0.146 mm; while accommodating pulsatile nature, the deformation needless to say increased to 0.40 mm which shows how much the pulsatile nature can influence the outcome of the physiological state of the ventricles.

5.5. Validation of the Results

Geometry of ventricles and tumor is segmented from subject-specific MRI datum and is also validated against the radiologist provided ground-truth. FSI framework is established on the walls of ventricle (the FSI surface) where exchange of data (forces and displacements) takes place between fluid and solid compartments. Structure-structure interaction is established between tumor and ventricle walls to apply tumor forces on the walls of CA. Tumor forces are grown in temporal spectrum using Gompertz mathematical model and are applied on the section area of CA to model stenosis. They are assumed to be applied in toto because herein we only aim to provide the fundamental framework to model such cases; and if and when such complete interactions (such as those coming from brain parenchyma) are considered, then the framework presented herein can be applied thereto with the difference of tumor forces magnitude on the walls of CA and inclusion of any other interactions as deemed necessary to consider. The proposed scheme considers all the relevant and major physiological factors which may significantly influence the CSF flow in the ventricles. These among others include dynamic interactions between the deformable wall of ventricles and CSF flow profiles. The role of CSF pulsatility is also catered in the proposed model to objectively show the readers that it has a noteworthy effect on the outcome of CSF flow, and on Transmantle pressures as also hinted by Holmlund et al [52-53] in their studies.

Table 4. Comparison of FSI results without and with tumor force application.

Parameters	**Without Tumor Force**	**With tumor Force (At 75% Stenosis level)**
Aqueduct Velocity (mm/s)	21.2	54.1
Ventricular walls Deformation (mm)	0.002	0.146
Pressure in Lateral Ventricles (Pa)	2.5	5.4
Pressure Drop in Cerebral Aqueduct (Pa)	1.7	5.3625

Table 6. Comparison of Results of Proposed Method to PC-MRI Studies reported in Literature

PC-MRI Study	Stroke volume (mL/beat) (±SD)	Peak velocity Craniocaudal cm/s (±SD)
Abbey et al (2009) [47]	0.017±0.010	3.24±1.08
Algin et al (2010) [48]	0.039±0.039	4.78±2.48
Lee et al (2004) [49]	0.02±0.0125	3.39±1.61
Proposed Method	0.006±0.01	Without tumor: 2.1 With tumor: 5.4

In the best of interest for readers, and to make them understand about the case of stenosis of CA, we have provided another set of simulation where we have compared the case of stenosis of CA to that of normal group wherein no tumor forces are applied and a simple FSI framework is

Table 5. Comparison of results from the Proposed Method to Previous FSI based Papers

Study	Velocity (mm/s) in CA	Pressure drop (Pa)	Deformation (mm)
Jacobson et al. (1996)	28	<1.1 for CA	Walls modeled as rigid
Fin and Grebe (2003)	64.65	2.91 for elastic wall model for CA	Implemented flexible cylindrical wall model of CA and obtained 0.61 mm deformation
Linninger et al. (2005)	25.8/-21.7	2 in CA	No deformation reported. However, net increase of ventricular volume of 4.5% is reported.
Kurtcuoglu et al (2005)	With 25% stenosis, velocity increased by 30%	With 25% stenosis, intraventricular pressure increased 8.9%	No deformation reported.
Kurtcuoglu et al. (2007)*	120	20	No deformation reported
Howden et al. (2008)	11.38	1.14	Walls modeled as rigid
Masoumi et al. (2010)	18/-15	<5	No deformation reported. However, net increase of ventricular volume of 6% is reported.
Masoumi et al. (2013)	8/-6	< 2	Normal CSF-Ventricular interaction: 0.006 mm
Proposed Framework	Without tumor interaction: 21.2 Stenosis of CA: 54.1	Without tumor interaction: 2.5 Stenosis of CA: 5.4	Without tumor interaction: 0.002 mm Stenosis of CA: 0.146 mm

*Note: Kurcuoglu (2007) reports velocity and pressure values which are not found elsewhere in the literature.

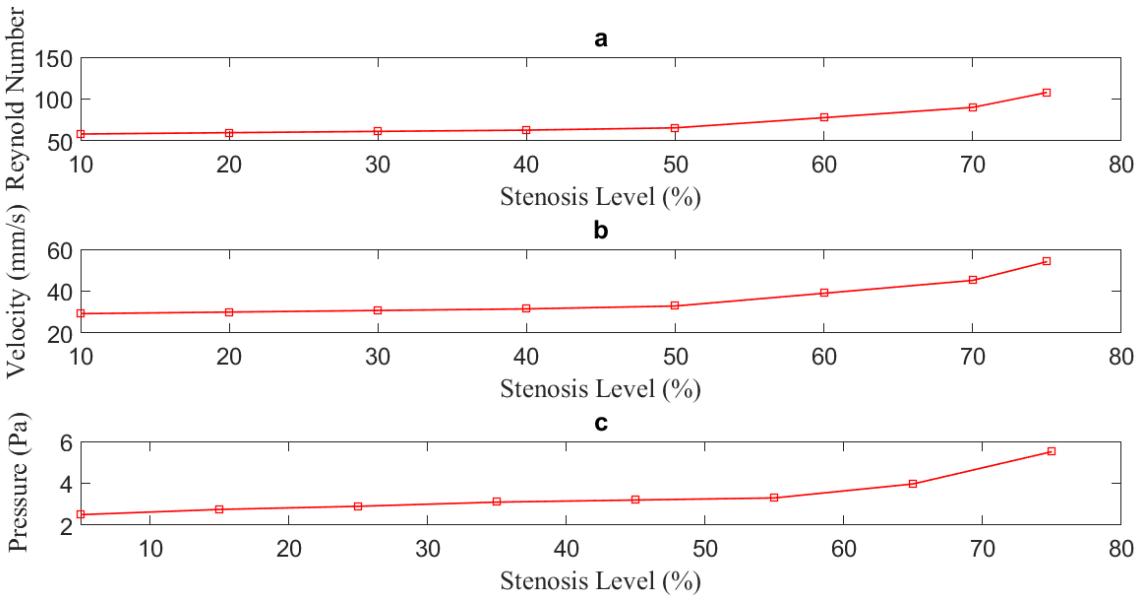

Figure 23. Flow parameters at various stenosis level (in percentage). (a) shows Reynold's Number against various levels of Stenosis; (b) shows velocity (in mm/s) in cerebral aqueduct against various levels of Stenosis; and (c) shows Pressure in lateral ventricles against various levels of Stenosis

implemented to observe usual deformation on the walls of ventricles. This comparison allows us to visualize inter-se differences and highlight the pathological difference between them in terms of aforenoted parameters. Table enlists this in succinct manner.

Validation of results is carried out via two independent sources. First, we have validated our results with past models of FSI presenting case studies of CSF flow parameters. This gives us a double check, even for both normal and stenosis case. Second source of validation are PC-MRI studies, taken from the literature, which provide experimental results for CSF flow parameters. Table 6 provides the results of present case and compares it with previous FSI-based papers (in terms of velocity, pressures and deformation, if any) and Table 7 provides PC-MRI studies reported in literature on either the same case of stenosis of CA or connected to it in some manner.

At various stenosis level (10-75%) graphs are plotted of velocity, pressure and Reynold's number which are provided in figure 23. As visible from figure 23 part (a), the velocity in initial stage starts to rise steadily until a level is reached where it changes abruptly and at 75% stenosis level it shoots upwards. Same goes with the Reynold's number (equation) as both have linear relationship (effective diameter of CA is 2 mm) and is provided in figure 23 part (b). Pressures in the lateral ventricles are presented via graph in figure 23 part (c). This graph is reminiscent of the graph usually found in intracranial pressure-volume graphs wherein after a critical point, pressure increases considerably in lateral ventricles because CSF accumulates. It is all the more obvious

that once retention of CSF has increased, pressure ought to increase especially in lateral ventricles because they are huge hollow cavities. Also, since obstruction occurs considerably, the outflow of CSF in fourth ventricle also gets disturbed and the flow increases towards lateral ventricles which is also visible in change in deformation of lateral ventricles (described above). Maximum local Reynold's number in the CA for normal group (where no tumor force is considered) well remains under 38.5 and under case of stenosis of CA it rises to 110. Local pressures on the walls of ventricle remain under 2.5 Pascals (0.018 mmHg) for normal control group which also well correlate with the reported values in literature (see table 6) hence strengthening the validation of model. Whereas for stenosis or near stenosis case (75% level), pressure increases up to 5.4 Pascals (0.040 mmHg). While for regions around the point of force application and fourth ventricle, pressure gradients are abrupt and change to negative pressures of maximum 10 Pa. This negative pressure suggests that near to obstruction of CSF, outflow to fourth ventricle has decreased thereby creating void around.

In addition, in determining the behavior of CSF inside cranium both in ventricles and subarachnoid space, Transmantle pressure is one variable which affects the outcome considerably. As discussed by Holmlund et al. [52-53] that in cases of ventriculomegaly, Transmantle pressures do increase under the influence of pulsatile nature of CSF in sections of CA. Our study has also positively concluded that the during stenosis of CA an increased Transmantle pressure is observed of twice the magnitude of that of normal case. Hence even in cases of ventriculomegaly or stenosis of CA, what our and Holmlund et al [52-53] study suggest is the fact that whenever constricted CSF flow (or under an inadequate CSF outflow) is observed the natural consequence thereof is the net increased Transmantle pressures on the ventricular body. Pulsatility may amplify that effect also in vortex formations et-cetera. Perhaps, the only difference between our study and Holmlund et al [52] is that of the absence of consideration ventricular wall movement in latter study which we believe have a considerable effect as detailed above when taken in conjunction with the pulsatile nature of CSF. Our study has provided a basic framework from which any ventricle-CSF interaction can be studied. Whether to include respiratory induced pulsations, backflow propagation of CSF in fourth ventricle, cases of non-communicating hydrocephalus, ventriculomegaly et-cetera all can not only be accommodated by using this framework presented herein but also may be improved and improvised to the more clinically realistic regimes. Hence, we believe that the proposed model (the two-way FSI) can easily capture not only those factors

which are documented in Holmlund et al [52] but also others as long as the focus and object of study is to unearth interactions of tissue in relation to ventricle-CSF interaction.

5.6. Relationship with Brain-Ventricular interaction and ICP

In cases of Stenosis of CA, the most common consequence of CSF obstruction is the resultant increase in ICP inside the cranium. In cases of hydrocephalus, ICP increases in similar manner. Thus, ICP can be understood as the net CSF pressure inside cranium. CSF pressure on walls of ventricles contribute significantly once stenosis occurs, especially on lateral ventricles due to blockage of CSF flow craniocaudal. Ergo, in this term, ICP can be directly related to CSF incremental pressures. However, in this case study, ventricle body is segregated from the integrated environment of brain interaction. As noted above, brain behaves as hyper-elastic, therefore, once pressures inside ventricle increase, those would contribute towards in expanding/deforming brain parenchyma significantly and net ICP (considering brain parenchyma as well) would increase drastically. Therefore, chapter 6 presents a case study wherein brain parenchyma interaction is also catered in the final mode. This collectively address both phase 3 and phase 4.

CHAPTER 6—RESULTS OF BRAIN PARENCHYMA INTERACTION AND ICP

Previous chapter enumerated results of simulation related to the FSI for ventricular body entailing flow of CSF. Now this chapter, which can be conveniently be termed as the heart and soul of this thesis, entails combining the results of previous chapter (which only considered FSI on ventricular body) to the ventricular-CSF-brain parenchyma interaction; only through this logical connection can we finally analyzed and produce a finite element model of ICP under the influence of tumor.

Case study 2—Brain Parenchyma interaction with tumor and CSF pressure

The FEM model on the structural side has 769322 elements, 678149 nodes and total number of 1707953 equations are solved, apart from additional contact element formulations. Fluid domain has 1144379 elements (tetrahedral). The model is solved on a supercomputer with 28 compute nodes consisting of 12 core Intel Xeon E5-2620 2.0 GHz processors and 48GB RAM on each node. Collective RAM requirements amount to 102 GB. The model simulation completed in 24 hours.

6.1. Brain Deformation Field

In this section I present the results of deformation field. Figure 24 (a-c) shows deformation in 3D view. Figure 25 (a-i) present cases of deformation under various timesteps. Figure 25 (a-c) show results of deformation evolution on the axial plane. Figure 25 (d-f) show deformation evolution on the sagittal cross section. Figure 25 (g-i) show deformation on the coronal cross section.

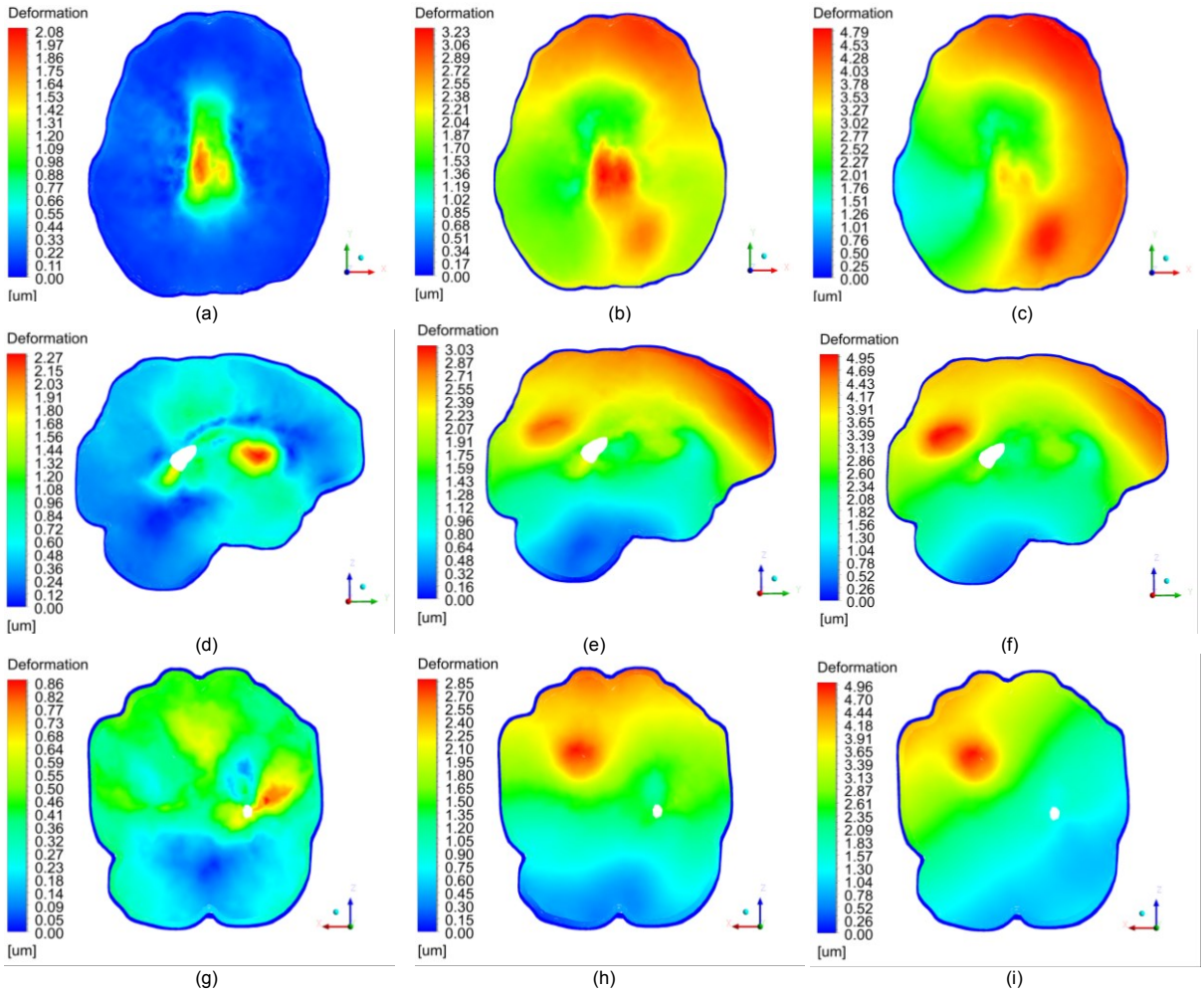

Figure 25. Deformation plot on axial, sagittal and coronal planes at different timesteps (0.1, 0.5 and 1 second). (a-c) shows deformation contour plot on axial plane at 0.1, 0.5 and 1 second respectively; (d-f) shows deformation contour plot on sagittal plane at 0.1, 0.5 and 1 second respectively; whereas, (g-i) shows deformation plot on coronal plane at 0.1, 0.5 and 1 second respectively

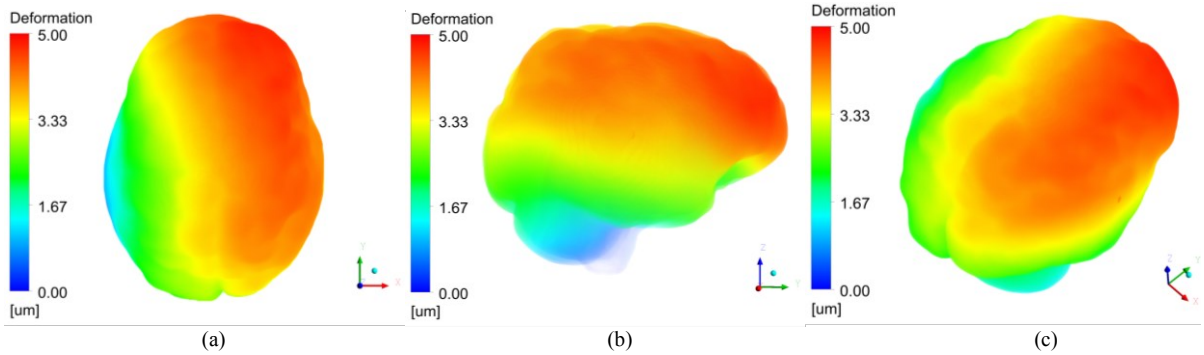

Figure 24. 3D Contour plot of deformation on the entire brain parenchyma. The contour plot is designed in such way wherein skull and any other layer which has zero deformation is made to appear to be transparent. The limits are appropriately scaled between 0-5 um. Herein (a) shows the top view of the deformation plot; (b) shows the side view of the deformation plot; whereas, (c) shows a tilted view

It is quite visible from figure 24 and figure 25 that the deformational impact of tumor on the brain parenchyma is significant. The impact actually travels all the way till the frontal lobe and if these results are read with the clinical stage of brain tumor, then they are pivotal. As noted in earlier part of thesis that I am dealing with an early instance tumor therefore, what transpires from these result is that if say a high grade glioma is present then that would carry in real and physical terms much greater deformation and may also accompany itself with midline brain shift. There are two ways to validate the results: By experimentation and finding results of tumor progress and brain deformation; or to record ICP values using Catheter inserted inside cranium.

Or by validating present results with any previous results (or even to relatable pathology) It is known to all and sundry that experimentation on the brain (for invasive cases) is not permitted and no human trials can even take place due to risky nature of trial (and is against ethical standards such as Helsinki Declaration). As for second point, as noted previously, literature is bereft of cases studying brain tumor interaction. And we can only remotely relate this point to the case for edema which comes at a cost since both pathologies have different set of assumption and biomechanical behavior. Notwithstanding aforementioned, according to paper by Fang Wang et al [117], for validation of brain deformation in a closed head model, there can only be two ways to do it: 1) validation of material properties (which has been done previously), (2) validation of boundary conditions which has also been done previously.

6.2. Stress field and ICP

Now we come to the aspect of stresses inside cranium. Figure 26 shows 3D contour plot of the stresses which are largely at the brain-CSF interface. This is expected as at the junction of these layers the compliance is expected therefore an expanding brain would necessarily create more stress at this brain barrier. Figure 27 shows the graph of von-mises, principal, shear stress and a normal ICP stress line is also plotted for comparison. ICP pressures inside cranium are found across the brain parenchyma at the brain-CSF interface. This is obvious since it is these two layers which have a meaningful interaction in terms of compliance. ICP of 10.81 mmHg is found which may appear to be in the normal range , however, since we are dealing with early brain tumor cases this is significant. Besides, according to a paper authored by Brian T. Andrews et al [118], the authors have conclusively shown that in presence of tumor, even at low ICP values (below 15

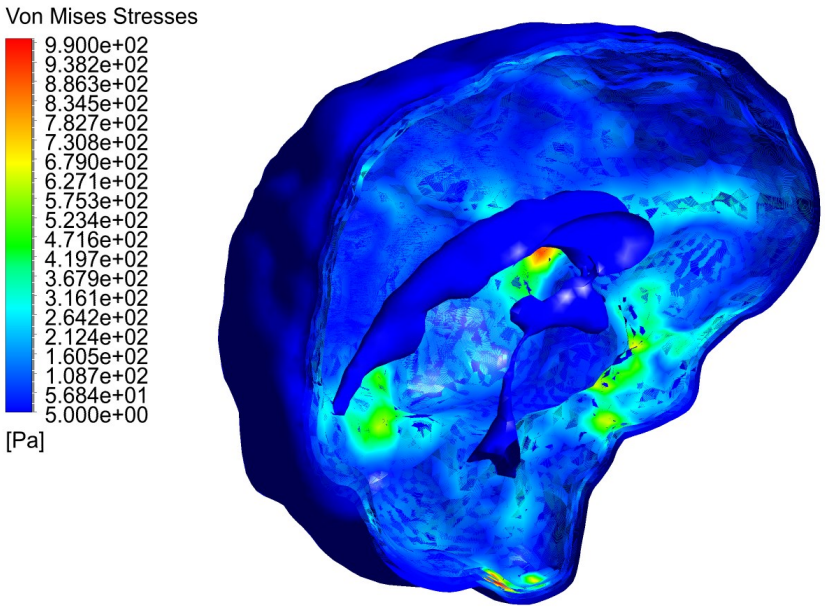

Figure 26. 3D Contour plot of stress

mmHg), herniation can occur. Furthermore, tumor's spatial location has a role to play. Jenny C. Kienzler et al [119], in their study have shown that the tumor in temporal region has a greater chance of brainstem compression than a tumor in frontal region. Furthermore, according to Bershard et al [120] the normal range of ICP (in his statistical study) was in the range of 11.5±4.5 mmHg. Hence this study is an attempt to model such effects non-invasively.

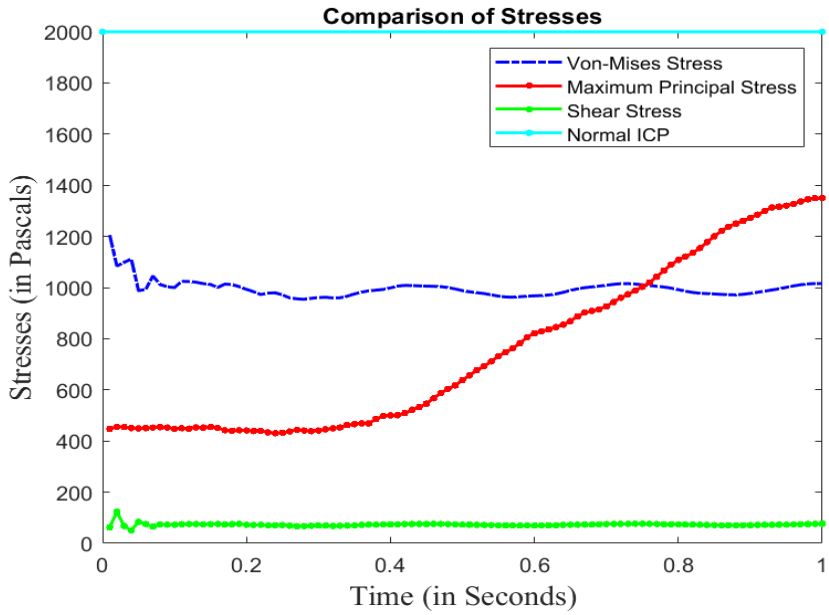

Figure 27. Stress Comparisons

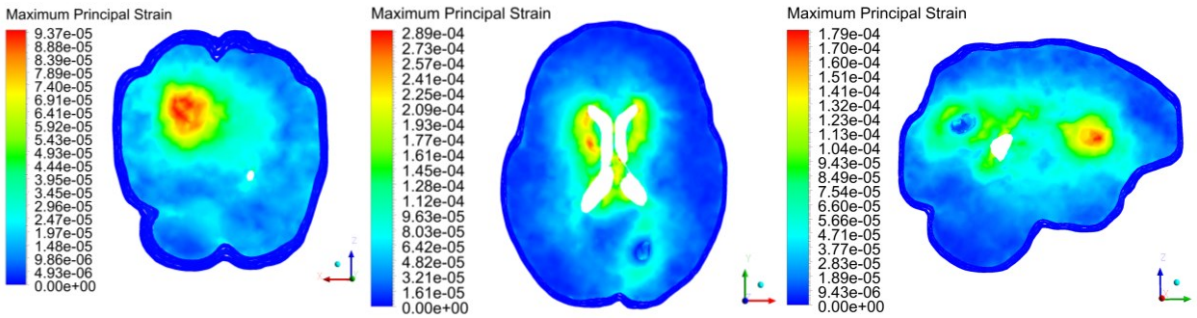

(a) (b) (c)

Figure 28. Contour plot of strain on (a) coronal, (b) axial and (c) sagittal view clearly highlighting the strain inside the cranium particularly around brain parenchyma.

6.3. Strain Distribution

Figure 28 (a-c) shows strain distribution on the coronal, axial and sagittal views. The strains are basically the changes in dimension of the brain parenchyma due to the tumor forces and as it is visible from graphs above that around the tumor region strain is evolving and increasing. Figure 29 shows the stain graphs. Strains are the direct implication of high deformation given above. Strain area localization is clearly around the tumor region where deformation is maximum.

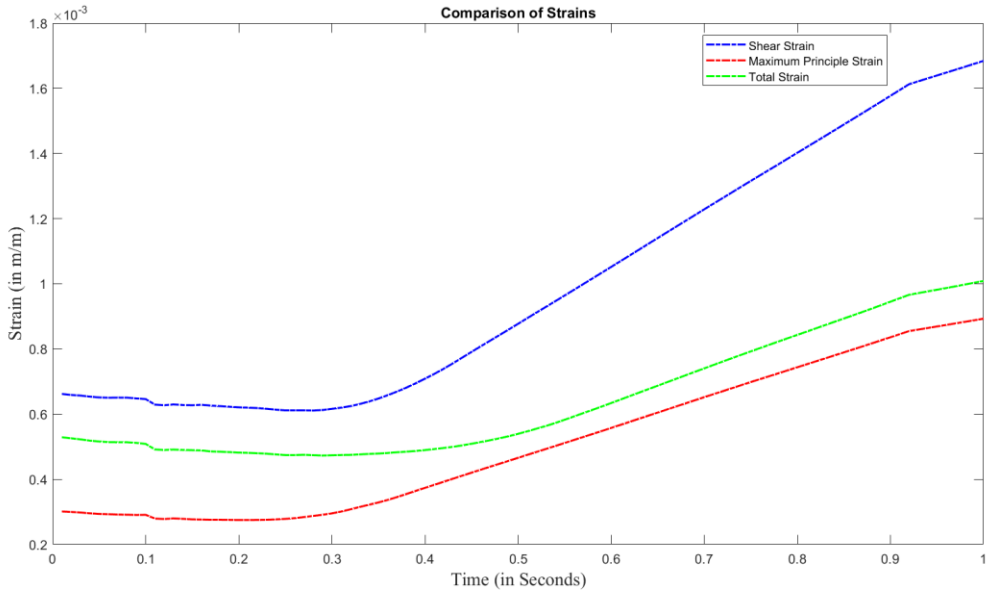

Figure 29. Strain comparisons

6.4. Synopsis and Contribution to Knowledge Base

This thesis has effectively modeled the ICP mechanics inside cranium while considering the interaction of tumor. This particular aspect has never been attended to in the literature. This is significant considering it adds to the already available knowledge base. From a holistic point of view following points can be summarized:

1. Novel Mapping of deformation progression and ICP on human brain when tumor is present.
2. A unique, anatomically realistic model in context to ICP mechanics in the literature has been studied.
3. The literature is almost bereft of any case study highlighting how tumor deformation progresses in long term (both for high-grade and low-grade tumor) over time.
4. This study has considered tumor in its early stages (because we need to study fundamentally how brain deformation pattern evolves in the earliest time of disease spread, i.e., tumor)

Lastly, where the biomedical engineering community stands at this particular problem, I think this study would definitely prove to be a quantum leap and a starting point in developing computational techniques to study in-vitro brain mechanics, especially ICP under various factors.

CHAPTER 7—CONCLUSION AND FUTURE WORK

Turning towards the end of this thesis, this chapter presents the conclusive findings of entire thesis in a very succinct and presentable form. It reiterates what assumptions have been made conclusion drawn thereof. It also presents some of the limitations of present work and also provides and presents areas for future works. First, as detailed in chapter 5, the ventricular body has role in the FSI simulation. If it is taken as rigid, then most of the interaction cannot be studied let alone calculated. Second, when considering the interaction of CSF with brain parenchyma then the role of ventricular wall in such case is pivotal. As noted earlier, taking ventricular wall as flexible is most suitable to study such interactions. Third, brain parenchyma modeling entails that it should be modelled as hyper-viscoelastic because its stress-strain response is highly non-linear and large strains are very much likely. Fourth, tumor has been grown mathematically using Gompertz mathematical model so that forces can be found out in time. These forces are non-linear in nature. Fifth, as noted in chapter 6, the brain parenchyma deformation response is highly dependent on both the CSF pressures and tumor. The maximum deformation goes up-to 5 um which when looked collectively (as this thesis only looks for early case tumor) then this is significant. Furthermore, there are additional factors at play as well therefore deformation is also susceptible when considering other factors. ICP inside cranium is found out to be 1442 Pascals (10.981 mmHg) which though within normal range; however since in this thesis, as noted previously, we are only dealing with an early tumor, such ICP is also significant. Next, I advert to some of the limitations of present study. First, it does not take into account the detailed structure of brain parenchyma. Meaning thereby that various sub-parenchyma layers are not considered—such as grey mater, white mater etc. Such inclusion of layers can be beneficial in overall analysis. Second, I have idealized tumor as a *solid core*. However, it has also some fluid hydrostatic forces which, if considered, may also improve standard model improvement. For future work, this thesis can prove to be a quantum leap in ascertaining the role of tumor interaction with brain parenchyma and ICP modeling. If aforenoted factors are also considered, then such model would be more accurate and robust.

REFERENCES

[1] J.D. Pickard, M. Czosnyka, "Management of raised Intracranial Pressure", Journal of Neurology, Neurosurgery and Psychiatry, Vol. 56, pp. 845-858, 1993.

[2] Q. T. Ostrom, G. Cioffi, H. Gittleman, N. Patil, K. Waite, C. Kruchko, et al., "CBTRUS statistical report: primary brain and other central nervous system tumors diagnosed in the United States in 2012–2016," Neuro-oncology, vol. 21, pp. v1-v100, 2019.

[3] R. L. Siegel, K. D. Miller, A. Goding Sauer, S. A. Fedewa, L. F. Butterly, J. C. Anderson, et al., "Colorectal cancer statistics, 2020," CA: a cancer journal for clinicians, 2020.

[4] Hydrocephalus Association. Hydrocephalus Facts and Stats. Retrieved from https://www.hydroassoc.org/about-us/newsroom/facts-and-stats-2/ accessed 14th August, 2019.

[5] W. E Arnould-Taylor, "A textbook of Anatomy and Physiology", 3rd edition, Stanley Thomas Publishers Ltd ,1977.

[6] Cinnamon VanPutte, Jennifer Regan and Andrew Russo, "Seeley's Essentials of Anatomy & Physiology", 9th edition, McGraw Hill Education, 2016.

[7] James Weyhenmeyer and Eve Gallman, "Rapid Review Neuroscience", Mosby Publishers, November 29, 2006.

[8] Ben L. C. Wright, James T. F. Lai and Alexandra J. Sinclair, "Cerebrospinal fluid and lumbar puncture: a practical review", Journal of Neurology, Volume 259, Issue 8, pp. 1530-1545, August 2012.

[9] Purves D, Augustine GJ, Fitzpatrick D, et al., editors, "The Neuroscience", second edition, Sunderland (MA): Sinauer Associates, 2001.

[10] L. A. Steiner and P.J.D. Andrews, "Monitoring the injured Brain: ICP and CBF", British Journal of Anaesthesia, Volume 97, Issue 1, pp. 26-38, July 2006.

[11] John M. Turner, "Intracranial Pressure", Book chapter in, "Textbook of Neuroanaesthesia and intensive care".

[12] Mokri B, "The Monro-Kellie hypothesis: applications in CSF volume depletion". Neurology. 56 (12): 1746–8, June 2001.

[13] Maya Harary, Rianne G.F. Dolmans and William B. Gormley, "Intracranial Pressure Monitoring—Review and Avenues for Development". Review article published in Sensors, 5 Feb 2018.

[14] P.H. Raboel, J. Bartek Jr., M. Andresen, B.M. Bellander and B. Romner, "Intracranial Pressure monitoring: Invasive versus Non-invasive Methods—A Review", Review article published in, "Critical Care Research and Practice", Vol 2012, Hindawi Publication Cooperation, March 2012.

[15] S.L. Battron, R.M. Chesnut, J. Ghajar et al., "Guidelines for the management of severe traumatic brain injury. VI. Indications for intracranial pressure monitoring", Journal of Neurotrauma, Vol. 24, supplement 1, pp. S37-S44, 2007.

[16] M. Smith, "Monitoring intracranial pressure in traumatic brain injury", Anaesthesia and Analgesia, Vol. 106, No. 1, pp. 240-248, 2008

[17] J. Bellner, B. Romner, P. Reinstrup, K. A. Kristiansson, E. Ryding and L. Brandt, "Transcranial Doppler sonography pulsating index (PI) reflects intracranial pressure (ICP)", Surgical Neurology, Vol. 62, no. 1, pp 45-51, 2004.

[18] N. J. Alperin, S. H. Lee, F. Loth, P. B. Raksin and T. Lichtor, "MR-intracranial pressure (ICP): a method to measure intracranial elastance and pressure non-invasively by of MR imaging: baboon and human study", Radiology, Vol. 217, no. 3, pp. 877-885, 2000.

[19] D. C. Collier, S. S. C. Burnett, M. Amin et al., "Assessment of consistency in contouring of normal-tissue anatomic structures", Journal of Applied Clinical Medical Physics, Vol. 4, Issue 1, pp. 17-24, 2003.

[20] F. Shi, D. Shen, P. T. Yap et al., "CENTS: Cortical enhanced neonatal tissue segmentation", Human Brain Mapping, Vol. 32, Issue 3, pp. 382-396, Published in Wiley, 2011.

[21] M. Prastawa, "An MRI segmentation framework for brains with anatomical deviations [Ph.D. thesis], University of North Carolina at Chapel Hill, 2007.

[22] M. Sezgin and B. Sankur, "Survey over image thresholding techniques and quantitative performance evaluation", Journal of Electronic Imaging, Vol. 13, Issue 1, pp. 146-168, 2004.

[23] T. Weglinski and A. Fabijanska, "Brain tumor segmentation from MRI data sets using region growing approach", in Proceedings of the 7th International Conference on Perspective Technologies and Methods in MEMS Design (MEMSTECH 11), pp. 185-188, May 2011.

[24] S. K. Warfield, F. A. Kaus, M. Jolesz and R. Kikinis, "Adaptive template moderated spatially varying classification", in Proceedings of the Medical Image Computing and Computer Assisted Intervention (MICCAI '98), pp. 431-438, 1998.

[25] P. Dhanalakshmi and T. Kanimozhi, "Automatic Segmentation of Brain tumor using K-Means Clustering and its Area Calculation", International Journal of Advanced Electrical and Electronics Engineering (IJAEEE), Vol. 2, Issue 2, pp. 2278-8948, ISSN (Print), 2013.

[26] M. N. Ahmed, S. M. Yamany, N. Mohamed, A. A. Farag and T. Moriarty, "A modified Fuzzy-C means algorithm for bias field estimation and segmentation of MRI data", in IEEE Transactions on Medical Imaging, Vol. 21, Issue 3, pp. 193-199, March 2002.

[27] Karim Kalti and Mohamed Ali Mahjoub, "Image segmentation by gaussian mixture models and modified FCM algorithm", International Arab Journal of Information and Technology, Vol. 11, Issue 1, January 2014.

[28] Ali M. Hasan, Farid Meziane, Rob Aspin and Hamid A. Jalab, "Segmentation of Brain Tumors in MRI Images Using Three-Dimensional Active Contour without Edge", Symmetry (Peer-reviewed Journal), Vol. 8, Issue 11, 2016.

[29] C. Baillard, P. Hellier and C. Barillot, "Segmentation of Brain 3D MR images using level sets and dense registration", Medical Image Analysis, Vol. 5, Issue 3, pp. 185-194, 2001.

[30] Sergio Pereira, Adriano Pinto, Victor Alves and Carlos A. Silva, “Brain Tumor Segmentation using Convolutional Neural Networks in MRI images”, IEEE Transactions on Medical Imaging, Vol. 35, Issue 5, pp. 1240-1251, 2016.

[31] Mohammad Havaei, Axel Davy, David Warde-Farley, Antoine Biard, Aaron Courville, Yoshua Bengio, Chris Pal, Pierre-Marc Jodoin and Hugo Larochelle, “Brain tumor segmentation with Deep Neural Networks”, Medical Image Analysis, Vol. 35, pp. 18-31, January 2017.

[32] Alexandre de Brébisson and Giovanni Montana, “Deep neural networks for anatomical brain segmentation”, Published in IEEE Conference on Computer Vision and Pattern Recognition Workshops (CVPRW), 2015.

[33] Torsten Rohlfing, Robert Brandt, Randolf Menzel, Daniel B. Russakoff, and Calvin R. Maurer, Jr., “Quo Vadis, Atlas-Based Segmentation”, Book Chapter Handbook of Biomedical Image Analysis, Volume III: Registration Models.

[34] Bruce Fischl, “FreeSurfer”, NeuroImage, Vol. 62, Issue 2, pp. 774-781, 15 August 2012.

[35] Rahul S. Desikan et al, “An automated labeling system for subdividing the human cerebral cortex on MRI scans into gyral based regions of interest”, NeuroImage, Volume 31, pp. 968-980, 2006.

[36] Christophe Destrieux, Bruce Fischl, Anders Dale and Eric Halgren, “Automatic parcellation of human cortical gyri and sulci using standard anatomical nomenclature”, NeuroImage, Volume 53, pp. 1-15, 2010.

[37] E. E. Jacobson, D. F. Fletcher, M. K. Morgan, and I. H. Johnston, "Fluid dynamics of the cerebral aqueduct," Pediatric neurosurgery, vol. 24, pp. 229-236, 1996.

[38] L. Fin and R. Grebe, "Three-dimensional modeling of the cerebrospinal fluid dynamics and brain interactions in the aqueduct of Sylvius," Computer methods in biomechanics and biomedical engineering, vol. 6, pp. 163-170, 2003.

[39] J. Tu, G. H. Yeoh, and C. Liu, Computational fluid dynamics: a practical approach: Butterworth-Heinemann, 2018.

[40] A. A. Linninger, C. Tsakiris, D. C. Zhu, M. Xenos, P. Roycewicz, Z. Danziger, et al., "Pulsatile cerebrospinal fluid dynamics in the human brain," IEEE Transactions on Biomedical Engineering, vol. 52, pp. 557-565, 2005.

[41] V. Kurtcuoglu, K. Jain, and B. A. Martin, "Modelling of cerebrospinal fluid flow by computational fluid dynamics," in Biomechanics of the Brain, ed: Springer, 2019, pp. 215-241.

[42] F. Loth, M. A. Yardimci, and N. Alperin, "Hydrodynamic modeling of cerebrospinal fluid motion within the spinal cavity," J. Biomech. Eng., vol. 123, pp. 71-79, 2001.

[43] L. Howden, D. Giddings, H. Power, A. Aroussi, M. Vloeberghs, M. Garnett, et al., "Three-dimensional cerebrospinal fluid flow within the human ventricular system," Computer methods in biomechanics and biomedical engineering, vol. 11, pp. 123-133, 2008.

[44] X. G. Li, H. von Holst, J. Ho and S. Kleiven, “3D Finite Element Modeling of Brain Edema: Initial Studies on Intracranial Pressure Using Comsol Multiphysics, Technical Papers and Presentation (COMSOL),

Published in 2009. <https://www.comsol.com/paper/3-d-finite-element-modeling-of-brain-edema-initial-studies-on-intracranial-press-6687> accessed 21st August, 2019.

[45] Zhaoxia Li and Yunhua Luo, "Finite Element Study of Correlation between Intracranial Pressure and External Vibration Responses of Human Head", Advances in Theoretical and Applied Mechanics, Vol. 3, Issue 3, pp. 139-149, 2010.

[46] Yunhua Luo, Zhaoxia Li & Hongxi Chen, "Finite-element study of Cerebrospinal fluid in mitigating closed head injuries", Proceedings of the Institution of Mechanical Engineers, Part H: Journal of Engineering in Medicine, pp. 499-509, May 10, 2012.

[47] Bin Yang, Kwong-Ming Tse, Ning Chen et al., "Development of a Finite Element Head Model for the Study of Impact Head Injury", BioMed Research International, Vol. 2014, Article ID 408278, 14 pages.

[48] N. Masoumi, F. Framanzad, B. Zamanian, A. Seddighi, M. Moosavi, S. Najarian, et al., "2D computational fluid dynamic modeling of human ventricle system based on fluid-solid interaction and pulsatile flow," Basic and clinical neuroscience, vol. 4, p. 64, 2013.

[49] Yukio Tada, Tatsuya Nagashima and Masanori Takada, "Biomechanics of Brain Tissue (Simulation of Cerebrospinal fluid), JSME International Journal, Series A, Vol. 37, Issue 2, 1994.

[50] Milan Toma & Paul D.H. Nguyen, "Fluid–structure interaction analysis of cerebrospinal fluid with a comprehensive head model subject to a rapid acceleration and deceleration", Brain Injury, Vol. 32, Issue 12, pp. 1576-1584, 2018. <DOI:10.1080/02699052.2018.1502470>

[51] S. Cheng, D. Fletcher, S. Hemley, M. Stoodley & L. Bilston, "Effects of fluid structure interaction in a three-dimensional model of the spinal subarachnoid space", Journal of Biomechanics, Vol. 47, Issue 11, pp. 2826-2830, 2014.

[52] B. H. Menze, A. Jakab, S. Bauer, J. Kalpathy-Cramer, K. Farahani, J. Kirby, et al., "The multimodal brain tumor image segmentation benchmark (BRATS)," IEEE transactions on medical imaging, vol. 34, pp. 1993-2024, 2014.

[53] K. Hirakawa, K. Hashizume, and T. Hayashi, "Viscoelastic property of human brain-for the analysis of impact injury (author's transl)," No to shinkei= Brain and nerve, vol. 33, p. 1057, 1981.

[54] Y. Li, J. Deng, J. Zhou, and X. Li, "Elastic and viscoelastic mechanical properties of brain tissues on the implanting trajectory of sub-thalamic nucleus stimulation," Journal of Materials Science: Materials in Medicine, vol. 27, p. 163, 2016.

[55] S. Budday, G. Sommer, G. Holzapfel, P. Steinmann, and E. Kuhl, "Viscoelastic parameter identification of human brain tissue," Journal of the mechanical behavior of biomedical materials, vol. 74, pp. 463-476, 2017.

[56] M. A. Calhoun, S. A. Bentil, E. Elliott, J. J. Otero, J. O. Winter, and R. B. Dupaix, "Beyond linear elastic modulus: viscoelastic models for brain and brain mimetic hydrogels," ACS Biomaterials Science & Engineering, vol. 5, pp. 3964-3973, 2019.

[57] J. E. L. Pacheco, C. A. Bavastri, and J. T. Pereira, "Viscoelastic relaxation modulus characterization using Prony series," Latin American Journal of Solids and Structures, vol. 12, pp. 420-445, 2015.

[58] L. Zhang, K. H. Yang, and A. I. King, "Comparison of brain responses between frontal and lateral impacts by finite element modeling," Journal of neurotrauma, vol. 18, pp. 21-30, 2001.

[59] C. Zhou, T. B. Khalil, and A. I. King, "A new model comparing impact responses of the homogeneous and inhomogeneous human brain," SAE transactions, pp. 2999-3015, 1995.

[60] W. Yan and O. D. Pangestu, "A modified human head model for the study of impact head injury," Computer methods in biomechanics and biomedical engineering, vol. 14, pp. 1049-1057, 2011.

[61] T. J. Horgan and M. D. Gilchrist, "Influence of FE model variability in predicting brain motion and intracranial pressure changes in head impact simulations," International Journal of Crashworthiness, vol. 9, pp. 401-418, 2004.

[62] F. Turquier, H. S. Kang, X. Trosseille, R. Willinger, F. Lavaste, C. Tarriere, et al., "Validation study of a 3D finite element head model against experimental data," SAE transactions, pp. 1912-1923, 1996.

[63] R. Willinger, H.-S. Kang, and B. Diaw, "Three-dimensional human head finite-element model validation against two experimental impacts," Annals of biomedical engineering, vol. 27, pp. 403-410, 1999.

[64] L. Shuck and S. Advani, "Rheological response of human brain tissue in shear," 1972.

[65] N. Yoganandan, F. A. Pintar, J. Zhang, and J. L. Baisden, "Physical properties of the human head: mass, center of gravity and moment of inertia," Journal of biomechanics, vol. 42, pp. 1177-1192, 2009.

[66] A. Al-Bsharat, "Computational analysis of brain injury [Ph. D. thesis]," Wayne State University, Detroit, Mich, USA, 2000.

[67] M. Salimi Jazi, A. Rezaei, G. Karami, F. Azarmi, and M. Ziejewski, "A computational study of influence of helmet padding materials on the human brain under ballistic impacts," Computer methods in biomechanics and biomedical engineering, vol. 17, pp. 1368-1382, 2014.

[68] C. Zhou, T. B. Khalil, and A. I. King, "A new model comparing impact responses of the homogeneous and inhomogeneous human brain," SAE transactions, pp. 2999-3015, 1995.

[69] Z. B. Redzic and M. B. Segal, "The structure of the choroid plexus and the physiology of the choroid plexus epithelium," Advanced drug delivery reviews, vol. 56, pp. 1695-1716, 2004.

[70] S. Benzekry, C. Lamont, A. Beheshti, A. Tracz, J. M. Ebos, L. Hlatky, et al., "Classical mathematical models for description and prediction of experimental tumor growth," PLoS Comput Biol, vol. 10, p. e1003800, 2014.

[71] H. Murphy, H. Jaafari, and H. M. Dobrovolny, "Differences in predictions of ODE models of tumor growth: a cautionary example," BMC cancer, vol. 16, pp. 1-10, 2016.

[72] A. Worschech, N. Chen, A. Y. Yong, Q. Zhang, Z. Pos, S. Weibel, et al., "Systemic treatment of xenografts with vaccinia virus GLV-1h68 reveals the immunologic facet of oncolytic therapy," BMC genomics, vol. 10, p. 301, 2009.

[73] S. Angeli, K. E. Emblem, P. Due-Tonnessen, and T. Stylianopoulos, "Towards patient-specific modeling of brain tumor growth and formation of secondary nodes guided by DTI-MRI," NeuroImage: Clinical, vol. 20, pp. 664-673, 2018.

[74] B. Yang, K.-M. Tse, N. Chen, L.-B. Tan, Q.-Q. Zheng, H.-M. Yang, et al., "Development of a finite element head model for the study of impact head injury," BioMed research international, vol. 2014, 2014.

[75] M. E. Wagshul, J. J. Chen, M. R. Egnor, E. J. McCormack, and P. E. Roche, "Amplitude and phase of cerebrospinal fluid pulsations: experimental studies and review of the literature," Journal of neurosurgery, vol. 104, pp. 810-819, 2006.

[76] C. K. Batchelor and G. Batchelor, An introduction to fluid dynamics: Cambridge university press, 2000.

[77] P. Young, S. Qidwai, A. Bagchi, N. Kota, C. Pearce, and R. Cotton, "Developing a finite element head model for impact simulation in Abaqus," in SIMULIA community conference, 2015.

[78] D. C. Viano, "Biomechanics of head injury—Toward a theory linking head dynamic motion, brain tissue deformation and neural trauma," SAE transactions, pp. 1070-1089, 1988.

[79] F. P. DiMasi, R. H. Eppinger, and F. A. Bandak, "Computational analysis of head impact response under car crash loadings," SAE transactions, pp. 3029-3042, 1995.

[80] A. M. Nahum, R. Smith, and C. C. Ward, "Intracranial pressure dynamics during head impact," SAE Technical Paper 0148-7191, 1977.

[81] J. S. Ruan, T. B. Khalil, and A. I. King, "Finite element modeling of direct head impact," SAE Technical Paper 0148-7191, 1993.

[82] L. Zhang, K. H. Yang, R. Dwarampudi, K. Omori, T. Li, K. Chang, et al., "Recent advances in brain injury research: a new human head model development and validation," SAE Technical Paper2001.

[83] M. Claessens, F. Sauren, and J. Wismans, "Modeling of the human head under impact conditions: a parametric study," SAE transactions, pp. 3829-3848, 1997.

[84] G. Belingardi, G. Chiandussi, and I. Gaviglio, "Development and validation of a new finite element model of human head," in Proc. 19th International Technical Conference of the Enhanced Safety of Vehicle (ESV), Washington, DC, 2005.

[85] C. Zhou, T. B. Khalil, and A. I. King, "A new model comparing impact responses of the homogeneous and inhomogeneous human brain," SAE transactions, pp. 2999-3015, 1995.

[86] L. Shuck and S. Advani, "Rheological response of human brain tissue in shear," 1972.

[87] Z. Zhou, X. Li, and S. Kleiven, "Fluid–structure interaction simulation of the brain–skull interface for acute subdural haematoma prediction," Biomechanics and modeling in mechanobiology, vol. 18, pp. 155-173, 2019.

[88] S. K. Zhou, D. Rueckert, and G. Fichtinger, "Computational biomechanics for medical image analysis" in *Handbook of medical image computing and computer assisted intervention*: Academic Press, 2019.

[89] Inmaculada C. Sorribes, Matthew N. J. Moore, Helen M. Byrne, and Harsh V. Jain, "A Biomechanical Model of Tumor-induced Intracranial Pressure and Edema in Brain Tissue", Biophysical Journal, Vol. 116, Issue 8, pp. 1560-1574, April 23, 2019.

[90] M. Ursino and C. A. Lodi, "A simple mathematical model of the interaction between intracranial pressure and cerebral hemodynamics", Journal of Applied Physiology Vol. 82, Issue 4, pp.1256–1269, 1997.

[91] Masoumi, N., Bastani, D., Najarian, S., Ganji, F., Farmanzad, F., & Seddighi, A. S. (2010). Mathematical modeling of CSF pulsatile hydrodynamics based on fluid–solid interaction. IEEE transactions on biomedical engineering, 57(6), 1255-1263.

[92] Kurtcuoglu, V., Soellinger, M., Summers, P., Boomsma, K., Poulikakos, D., Boesiger, P., & Ventikos, Y. (2007). Computational investigation of subject-specific cerebrospinal fluid flow in the third ventricle and aqueduct of Sylvius. Journal of biomechanics, 40(6), 1235-1245.

[93] Abbey, P., Singh, P., Khandelwal, N., & Mukherjee, K. K. (2009). Shunt surgery effects on cerebrospinal fluid flow across the aqueduct of Sylvius in patients with communicating hydrocephalus. Journal of Clinical Neuroscience, 16(4), 514-518.

[94] Algin, O., Hakyemez, B., & Parlak, M. (2010). The efficiency of PC-MRI in diagnosis of normal pressure hydrocephalus and prediction of shunt response. Academic radiology, 17(2), 181-187.

[95] Lee, J. H., Lee, H. K., Kim, J. K., Kim, H. J., Park, J. K., & Choi, C. G. (2004). CSF flow quantification of the cerebral aqueduct in normal volunteers using phase contrast cine MR imaging. Korean journal of radiology, 5(2), 81-86.

[96] Siyahhan, B., Knobloch, V., de Zélicourt, D., Asgari, M., Schmid Daners, M., Poulikakos, D., & Kurtcuoglu, V. (2014). Flow induced by ependymal cilia dominates near-wall cerebrospinal fluid dynamics in the lateral ventricles. Journal of the Royal Society Interface, 11(94), 20131189.

[97] P. Holmlund, S. Qvarlander, J. Maim, and A. Eklund, "Can pulsatile CSF flow across the cerebral aqueduct cause ventriculomegaly? A prospective study of patients with communicating hydrocephalus," Fluids and Barriers of the CNS, vol. 16, pp. 1-10, 2019.

[98] P. Holmlund, "Fluid dynamic principles for analysis of intracranial pressure control: application towards space medicine and hydrocephalus," Umeå Universitet, 2019.

[99] Darvish, K. K., & Crandall, J. R. (2001). Nonlinear viscoelastic effects in oscillatory shear deformation of brain tissue. Medical engineering & physics, 23(9), 633-645.

[100] Tan, K., Cheng, S., Jugé, L., & Bilston, L. E. (2013). Characterising soft tissues under large amplitude oscillatory shear and combined loading. Journal of biomechanics, 46(6), 1060-1066.

[101] Sahoo, D., Deck, C., & Willinger, R. (2014). Development and validation of an advanced anisotropic visco-hyperelastic human brain FE model. journal of the mechanical behavior of biomedical materials, 33, 24-42.

[102] Kaster, T., Sack, I., & Samani, A. (2011). Measurement of the hyperelastic properties of ex vivo brain tissue slices. Journal of biomechanics, 44(6), 1158-1163.

[103] Laksari, K., Shafieian, M., & Darvish, K. (2012). Constitutive model for brain tissue under finite compression. Journal of biomechanics, 45(4), 642-646.

[104] Mihai, L. A., Budday, S., Holzapfel, G. A., Kuhl, E., & Goriely, A. (2017). A family of hyperelastic models for human brain tissue. Journal of the Mechanics and Physics of Solids, 106, 60-79.

[105] Rashid, B., Destrade, M., & Gilchrist, M. D. (2014). Mechanical characterization of brain tissue in tension at dynamic strain rates. Journal of the mechanical behavior of biomedical materials, 33, 43-54.

[106] Chatelin, S., Deck, C., & Willinger, R. (2013). An anisotropic viscous hyperelastic constitutive law for brain material finite-element modeling. Journal of biorheology, 27(1-2), 26-37.

[107] Hosseini-Farid, M., Ramzanpour, M., Ziejewski, M., & Karami, G. (2019). A compressible hyper-viscoelastic material constitutive model for human brain tissue and the identification of its parameters. International Journal of Non-Linear Mechanics, 116, 147-154.

[108] Rashid, B., Destrade, M., & Gilchrist, M. D. (2012). Mechanical characterization of brain tissue in compression at dynamic strain rates. Journal of the mechanical behavior of biomedical materials, 10, 23-38.

[109] Levental, I., Georges, P. C., & Janmey, P. A. (2007). Soft biological materials and their impact on cell function. Soft Matter, 3(3), 299-306.

[110] Pogoda, K., Chin, L., Georges, P. C., Byfield, F. J., Bucki, R., Kim, R., ... & Janmey, P. A. (2014). Compression stiffening of brain and its effect on mechanosensing by glioma cells. New journal of physics, 16(7), 075002.

[111] Tan, K., Cheng, S., Jugé, L., & Bilston, L. E. (2013). Characterising soft tissues under large amplitude oscillatory shear and combined loading. Journal of biomechanics, 46(6), 1060-1066.

[112] Miller, K., & Chinzei, K. (2002). Mechanical properties of brain tissue in tension. Journal of biomechanics, 35(4), 483-490.

[113] Lubarda, V. A. (2004). Constitutive theories based on the multiplicative decomposition of deformation gradient: Thermoelasticity, elastoplasticity, and biomechanics. Appl. Mech. Rev., 57(2), 95-108.

[114] Vujošević, L., & Lubarda, V. A. (2002). Finite-strain thermoelasticity based on multiplicative decomposition of deformation gradient. Theoretical and applied mechanics, (28-29), 379-399.

[115] Ogden, R. W. (1972). Large deformation isotropic elasticity–on the correlation of theory and experiment for incompressible rubberlike solids. Proceedings of the Royal Society of London. A. Mathematical and Physical Sciences, 326(1567), 565-584.

[116] Wittek, A., Miller, K., Kikinis, R., & Warfield, S. K. (2007). Patient-specific model of brain deformation: Application to medical image registration. Journal of biomechanics, 40(4), 919-929.

[117] F. Wang et al., "Prediction of brain deformations and risk of traumatic brain injury due to closed-head impact: quantitative analysis of the effects of boundary conditions and brain tissue constitutive model," vol. 17, no. 4, pp. 1165-1185, 2018.

[118] B. T. Andrews, B. W. Chiles, W. L. Olsen, and L. H. J. J. o. n. Pitts, "The effect of intracerebral hematoma location on the risk of brain-stem compression and on clinical outcome," vol. 69, no. 4, pp. 518-522, 1988.

[119] J. C. Kienzler, R. Zakelis, S. Bäbler, E. Remonda, A. Ragauskas, and J. J. O. N. Fandino, "Validation of noninvasive absolute intracranial pressure measurements in traumatic brain injury and intracranial hemorrhage," vol. 16, no. 2, pp. 186-196, 2019.

[120] E. M. Bershad et al., "Clinical validation of a transcranial Doppler-based noninvasive intracranial pressure meter: a prospective cross-sectional study," vol. 89, pp. 647-653. e1, 2016.